European Journal of Medicinal Chemistry 112 (2016) 114–129

Contents lists available at ScienceDirect

European Journal of Medicinal Chemistry

journal homepage: http://www.elsevier.com/locate/ejmech

Research paper

Discovery of antitumor anthra[2,3-*b*]furan-3-carboxamides: Optimization of synthesis and evaluation of antitumor properties

Andrey E. Shchekotikhin [a, b, *], Lyubov G. Dezhenkova [a], Vladimir B. Tsvetkov [c, d], Yuri N. Luzikov [a], Yulia L. Volodina [e], Victor V. Tatarskiy Jr. [e], Anastasia A. Kalinina [e], Michael I. Treshalin [a], Helen M. Treshalina [e], Vladimir I. Romanenko [e], Dmitry N. Kaluzhny [f], Michael Kubbutat [g], Dominique Schols [h], Yves Pommier [i], Alexander A. Shtil [a, e], Maria N. Preobrazhenskaya [a, 1]

[a] *Gause Institute of New Antibiotics, 11 B. Pirogovskaya Street, Moscow 119021, Russia*
[b] *Mendeleyev University of Chemical Technology, 9 Miusskaya Square, Moscow 125190, Russia*
[c] *Topchiev Institute of Petrochemical Synthesis, Russian Academy of Sciences, 29 Leninsky Avenue, 119991 Moscow, Russia*
[d] *Institute for Physical-Chemical Medicine, 1A M. Pirogovskaya Street, Moscow 119435, Russia*
[e] *Federal State Budgetary Scientific Institution «N.N. Blokhin Cancer Research Center» of the Ministry of Health of the Russian Federation, 24 Kashirskoye Shosse, Moscow 115478, Russia*
[f] *Engelhardt Institute of Molecular Biology, Russian Academy of Sciences, 32 Vavilov Street, Moscow 119991, Russia*
[g] *ProQinase GmbH, Breisacher Str. 117, 79106 Freiburg, Germany*
[h] *Rega Institute for Medical Research, KU Leuven, 3000 Leuven, Belgium*
[i] *Developmental Therapeutics Branch, National Cancer Institute, NIH, 37 Convent Drive, 37-5068, Bethesda, MD 20892, USA*

ARTICLE INFO

Article history:
Received 30 October 2015
Received in revised form
27 January 2016
Accepted 28 January 2016
Available online 4 February 2016

We dedicate this work to the memory of Professor Maria N. Preobrazhenskaya, the eminent scholar in bioorganic and medicinal chemistry.

Keywords:
Anthra[2,3-*b*]furan-3-carboxamides
DNA ligands
Topoisomerase inhibitors
Protein kinase inhibitors
Cytotoxicity
Circumvention of multidrug resistance
Antitumor activity

ABSTRACT

Anthraquinones and their analogues, in particular heteroarene-fused anthracendiones, are prospective scaffolds for new compounds with improved antitumor characteristics. We herein report the use of a 'scaffold hopping' approach for the replacement of the core structure in the previously discovered hit compound naphtho[2,3-*f*]indole-5,10-dione **2** with an alternative anthra[2,3-*b*]furan-5,10-dione scaffold. Among 13 newly synthesized derivatives the majority of 4,11-dihydroxy-2-methyl-5,10-dioxoanthra[2,3-*b*]furan-3-carboxamides demonstrated a high antiproliferative potency against a panel of wild type and drug resistant tumor cell lines, a property superior over the reference drug doxorubicin or lead naphtho[2,3-*f*]indole-5,10-dione **2**. At low micromolar concentrations the selected derivative of (*R*)-3-aminopyrrolidine **3c** and its stereoisomer (*S*)-3-aminopyrrolidine **3d** caused an apoptotic cell death preceded by an arrest in the G2/M phase. Studies of intracellular targets showed that **3c** and **3d** formed stable intercalative complexes with the duplex DNA as determined by spectral analysis and molecular docking. Both **3c** and **3d** attenuated topoisomerase 1 and 2 mediated unwinding of the supercoiled DNA via a mechanism different from conventional DNA-enzyme tertiary complex formation. Furthermore, **3d** decreased the activity of selected human protein kinases *in vitro*, indicating multiple targeting by the new chemotype. Finally, **3d** demonstrated an antitumor activity in a model of murine intraperitoneally transplanted P388 leukemia, achieving the increase of animal life span up to 262% at tolerable doses. Altogether, the 'scaffold hopping' demonstrated its productivity for obtaining new perspective antitumor drug candidates.

1. Introduction

Along with the advance of targeted anticancer therapy, the anthracycline antibiotics and their synthetic analogues remain highly effective drugs applicable in many chemotherapeutic schedules [1]. However, the clinical use of these drugs including the 'gold standard' doxorubicin **1** (Fig. 1) is frequently limited by organ

Abbreviations: CDI, 1,1′-carbonyldiimidazole; DCC, *N,N′*-dicyclohexylcarbodiimide; EDC, 1-ethyl-3-(3-dimethylaminopropyl)carbodiimide; FITC, fluorescein isothiocyanate; PyBOP, benzotriazol-1-yl-oxytripyrrolidinophosphonium hexafluorophosphate; HATU, 1-[bis(dimethylamino)methylene]-1*H*-1,2,3-triazolo[4,5-*b*]pyridinium 3-oxide hexafluorophosphate; PI, propidium iodide; TBTU, O-(benzotriazol-1-yl)-*N,N,N′,N′*-tetramethyluronium tetrafluoroborate.

* Corresponding author. Gause Institute of New Antibiotics, 11 B. Pirogovskaya Street, Moscow 119021, Russia.
E-mail address: shchekotikhin@mail.ru (A.E. Shchekotikhin).

[1] Deceased author.

http://dx.doi.org/10.1016/j.ejmech.2016.01.050
0223-5234/

toxicity (mostly heart and bone marrow) and altered drug response. Therefore, studies of new anthracyclines and their analogues with improved chemotherapeutic properties are underway [2]. Next generations of anthracycline based drug candidates have been evaluated in preclinical or clinical studies [3–7].

A variety of chemical modifications have been performed to identify the compounds with defined intracellular targets, decreased general toxicity and circumvention of drug resistance. The most important structural moiety responsible for therapeutic properties of anthracyclines is the anthraquinone core. Therefore, anthraquinones and their analogues are widely used as scaffolds for the design of anticancer drug candidates. Previously we have identified a high potential of hydroxy and amino derivatives of linear hetareneanthracendiones. In particular, a series of pyrrole, furan and thiophene fused derivatives of anthracendione that target duplex or quadruplex DNA, have been designed and evaluated [8–10]. 3-Aminomethylnaphtho[2,3-*f*]indole-5,10-diones with cyclic diamines in the side chain demonstrated a potent inhibition of DNA modifying enzymes topoisomerases 1 and 2 (Top1, Top2) and a high cytotoxicity against wild type and drug resistant tumor cell lines [11,12]. The selected compound **2** (Fig. 1) demonstrated a superior cytotoxicity than the reference drug **1** against mammalian tumor cell lines with determinants of altered drug response (such as Pgp expression or p53 inactivation) as well as promising therapeutic efficacy *in vivo* [12]. However, further development of 3-aminomethylnaphtho[2,3-*f*]indole-5,10-diones is limited by a multistep procedure of synthesis.

In search for more accessible analogues we focused on the core structure replacement ('scaffold hopping') [13]. Our previous studies identified two important moieties of 3-aminomethylnaphtho[2,3-*f*]indole-5,10-diones, namely, a cyclic diamine as a side chain in the position 3 (3-aminopyrrolidine residue in **2**) and hydroxyl groups in the peri-position (4, 11) in the quinone fragment of the core structure. Removal or modifications of these moieties decreased the antiproliferative potency of naphtho[2,3-*f*]indole-5,10-diones. Based on these results, the 'scaffold hopping' approach was employed to obtain new hetarenanthracenediones.

In this study we replaced the core structure of naphtho[2,3-*f*]indole-5,10-dione **2** with an alternative anthra[2,3-*b*]furan-5,10-dione scaffold (Fig. 2) and analyzed the properties of new compounds as antitumor drug candidates. Given its accessibility and potential for diversification, 4,11-dihydroxy-2-methyl-5,10-dioxoanthra[2,3-*b*]furan-3-carboxylic acid can be considered an attractive scaffold. Transformation of this acid into the amides bearing cyclic diamine residues yielded anthra[2,3-*b*]furan-3-carboxamides highly similar to 3-aminomethylnaphtho[2,3-*f*]indole-5,10-diones. We hypothesized that compounds with this scaffold retain the major properties critical for cytotoxicity of anthraquinones, i.e., the ability to bind to the double stranded DNA and inhibit topoisomerases. Additionally, the scaffold hopping led to the modification of the methylene spacer in 3-aminomethylnaphtho[2,3-*f*]indole-5,10-diones into the carboxamide group at the appropriate position on the new scaffolds (Fig. 2), providing an opportunity for drug binding to intracellular targets.

The 'scaffold hopping' drug design strategy helped to identify a new class of potential antitumor agents with the accessible scaffold. The naphtho[2,3-*f*]indole-5,10-dione **2** was synthesized via a linear scheme that included 11 stages whereas the analogues **3a**–**m** based on anthra[2,3-*b*]furan-5,10-dione scaffold can be obtained in 4–5 steps starting from commercially available quinizarine.

Presented herein is the design, synthesis and antitumor characteristics of a new class of antitumor agents based on anthra[2,3-*b*]furan-3-carboxamides with cyclic diamine moieties attached to carboxamide function. The combination of synthetic methods with 'scaffold hopping' approach led to the discovery of **3d** with improved properties *in vitro* and *in vivo*.

2. Results and discussion

2.1. Chemistry

At the initial step of synthesis of a new series of 4,11-dihydroxy-2-methyl-5,10-dioxoanthra[2,3-*b*]furan-3-carboxamides, the starting anthra[2,3-*b*]furan-3-carboxylic acid was obtained. According to the method of preparation of 4,11-dihydroxy-2-methyl-5,10-dioxoanthra[2,3-*b*]furan-3-carboxylic acid (**6**) [14], the condensation of ethyl acetoacetate with 1,4-hydroxy-2,3-dichloroanthraquinone (**4a**) led to ethyl 4,11-dihydroxy-2-methyl-5,10-dioxoanthra[2,3-*b*]furan-3-carboxylate (**5a**, Scheme 1). The ester **5a** is rather stable to alkaline or acidic hydrolysis, so for its cleavage to anthra[2,3-*b*]furan-3-carboxylic acid **6** a severe heating in concentrated sulphuric acid was used. With this method the efficacy of synthesis of **6** was limited. Mainly, we achieved only 38–42% yield of **5a** compared to 58% in the original procedure [14]. Furthermore, the harsh conditions, big consumption of sulphuric acid for hydrolysis of **5a**, and an insufficient purity of the target acid **6** were disadvantageous.

Therefore, for preparative synthesis of **6** we modified the reported procedure. For heterocyclization we used a more reactive 2,3-dibromoquinizarine **4b** [15] and *tert*-butyl acetoacetate. The addition of the base into the reaction mixture at 120–125 °C increased the yield of **5b** and improved its purity by reducing the formation of tar and angular by-products of heterocyclization. This optimization elevated the yield of *tert*-butyl ester **5b** up to 68% and

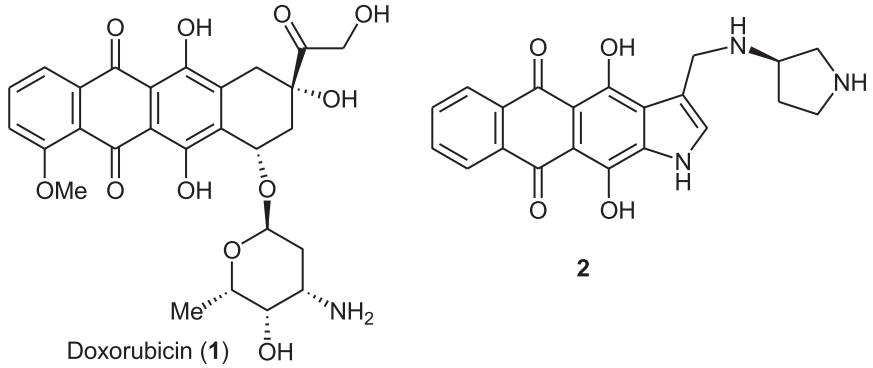

Fig. 1. Structures of doxorubicin (**1**) and lead naphtho [2,3-*f*]indole-5,10-dione **2**.

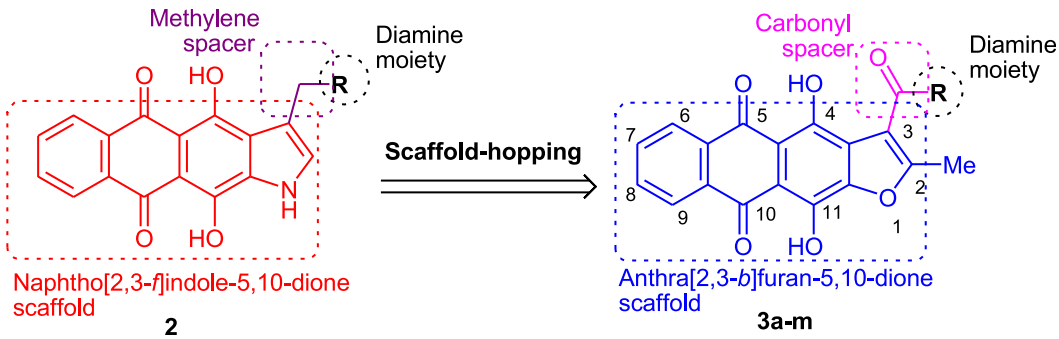

Fig. 2. 'Scaffold hopping': from 3-aminomethyl-4,11-dihydroxynaphtho [2,3-*f*]indole-5,10-dione **2** to 4,11-dihydroxy-2-methyl-5,10-dioxoanthra [2,3-*b*]furan-3-carboxamides **3a**–**m**.

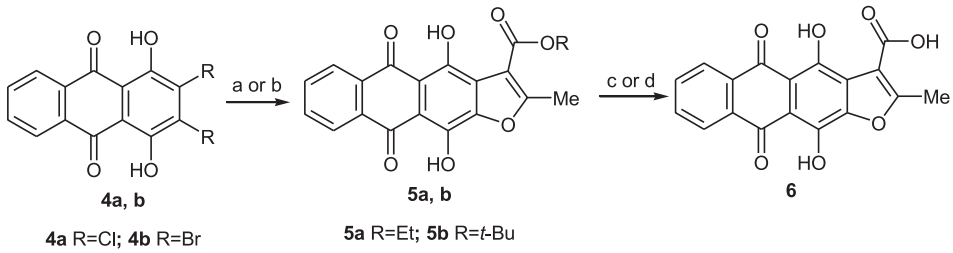

Scheme 1. Synthesis of 4,11-dihydroxy-2-methyl-5,10-dioxoanthra [2,3-*b*]furan-3-carboxylic acid (**6**). Reagents and conditions: (a) ethyl acetoacetate, K_2CO_3, DMSO, 125 °C, 1.5 h, 35% **5a** from **4a**; (b) *tert*-butyl acetoacetate, K_2CO_3, DMSO, 125 °C, 15 min, 68% **5b** from **4b**; (c) H_2SO_4, 110 °C, 1 h, 84% **6** from **5a** (d) trifluoroacetic acid, $CHCl_3$, RT, 2 h, 97% **6** from **5b**.

simplified its isolation and purification. Cleavage of tertiary ester **5b** proceeded easier than of ethyl ester **5a**, so a weak acid can be used for hydrolysis. Thus, treatment of **5b** with trifluoroacetic acid gave anthra[2,3-*b*]furan-3-carboxylic acid **6** in a quantitative yield with high purity.

For transformation of **6** into anthra[2,3-*b*]furan-3-carboxamides, we tested various methods of activation of the carboxyl group, including treatment with CDI, carbodiimides DCC or EDC and condensing agents PyBOP, HATU and TBTU. These methods yielded too small amounts of carboxamide (5–25%). The most efficient approach to activate the carboxyl group in **6** was the transformation into acyl chloride **7** by treatment with thionyl chloride in refluxing benzene (Scheme 2). Compound **7** was unstable during storage, although treatment of freshly prepared **7** with amines gave the corresponding carboxamides in high yields. To obtain anthra[2,3-*b*]furan-3-carboxamides **3a**–**k** the corresponding mono-Boc protected cyclic diamines were used. Intermediate Boc-carboxamides were purified by column chromatography and converted into target derivatives **3a**–**k** in a good yield (59–76%). Initially, a 3 M solution of HCl in methanol was used for deprotection; however, the resulting hydrochlorides were poorly soluble in water. Therefore, methanesulphonic acid was used for deprotection and the resulting methanesulphonates of anthra[2,3-*b*]furan-3-carboxamides **3a**–**k** showed a better water solubility. The carboxamides **3l**,**m** with the tertiary amino group in the side chain were obtained by acylation of methylpiperazine or 3-aminoquinuclidine and converted into water soluble mesylates.

The target compounds **3a**–**m** were further purified by chromatography and re-precipitation of their mesylate salts. The purified compounds were used for analytical and biological studies. The analytical and spectroscopic data of **3a**–**m** were in full accordance with assigned structures. Of note, significant dynamic changes were observed in NMR spectra of **3a**–**m**. Thus, at room temperature in ^{1}H NMR spectrum of **3d** the signals of the chromophore were slightly broadened; for diamine residues a double set of broadened signals was observed (Fig. S1). In ^{13}C NMR spectra of anthra[2,3-*b*]furan-3-carboxamides at room temperature the signals of carbon atoms of the chromophore frequently duplicated. The signals of C atoms of diamine residues were significantly broadened (Fig. S2). The signals in ^{1}H and ^{13}C NMR spectra were liable for shifting and exhibited a coalescence behavior in the temperature range 105–130 °C (Figs. S1–S2). At 107 °C the pairs of the signals of C atoms of the aromatic part of **3d** in ^{13}C NMR spectra coalesced in one accidental signal. These changes were accompanied by a decreased width of signals of the diamine moiety whose C atoms were observed as duplicated signals even at 135 °C. Dynamic changes of anthra[2,3-*b*]furan-3-carboxamides can be explained by hampered conformational interconversions of the diamine moiety due to rotational barriers in the carboxamide spacer attached to the chromophore's side chain. In **3a**–**f**, **j**, **k**, **m** bearing asymmetrical diamines in the side chains the barrier to CO–N rotation in amides [16] can lead to the formation of geometrical isomers (*E*/*Z*) conversable into each other (Scheme 3).

This explanation fits the observed duplication of signals of carbon atoms in ^{13}C NMR spectra of anthra[2,3-*b*]furan-3-carboxamides at low temperatures and their coalescence during heating. Furthermore, in **3a**–**m** the rotation of the Het–CON bond is restricted due to steric hindrance between the carboxamide moiety and the substituents in positions 2 and 4 (methyl and hydroxyl groups). This type of rotation restriction yields atropisomers in sterically hindered tertiary aromatic amides [17,18]. Thus, NMR spectroscopy data strongly suggested that anthra[2,3-*b*]furan-3-carboxamides **3a**–**f**, **j**, **k**, **m** with chiral diamines in their side chains represent a mixture of *E*/*Z* isomers or rotamers able to reversibly convert into each other.

2.2. Biological testing

2.2.1. Antiproliferative activity

The antiproliferative potency of mesylates of 4,11-dihydroxy-2-

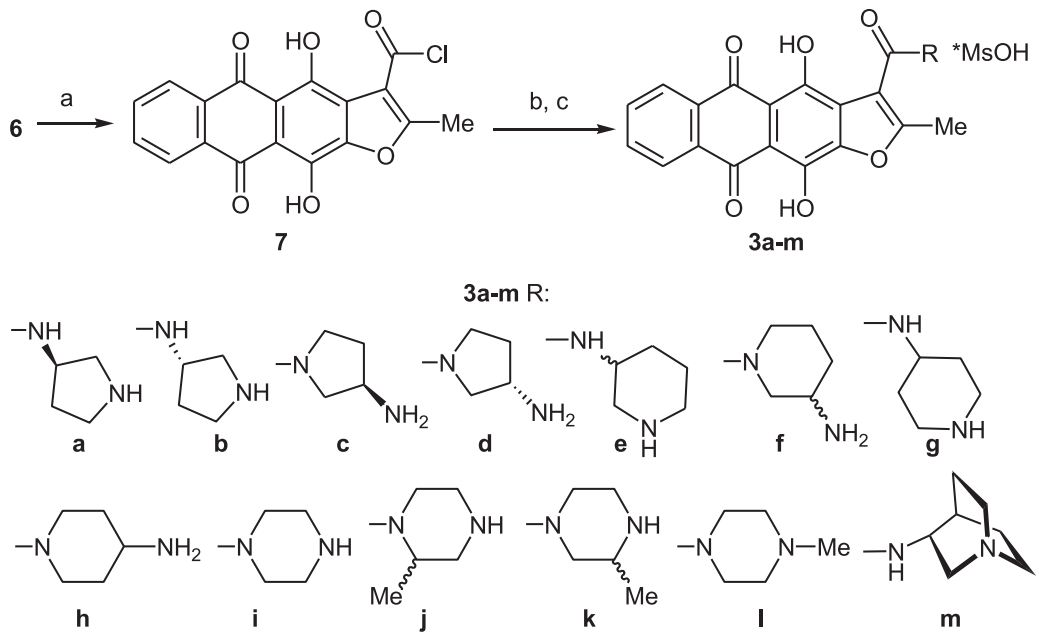

Scheme 2. Synthesis of 4,11-dihydroxy-2-methyl-5,10-dioxoanthra [2,3-*b*]furan-3-carboxamides **3a**–**m**. Reagents and conditions: (a) $SOCl_2$, PhH, reflux, 1 h; (b) HR (*N*-Boc protected diamine or diamine), Py, $CHCl_3$, RT, reflux, 5 min; (c) MsOH, $CHCl_3$, RT, 59–76%.

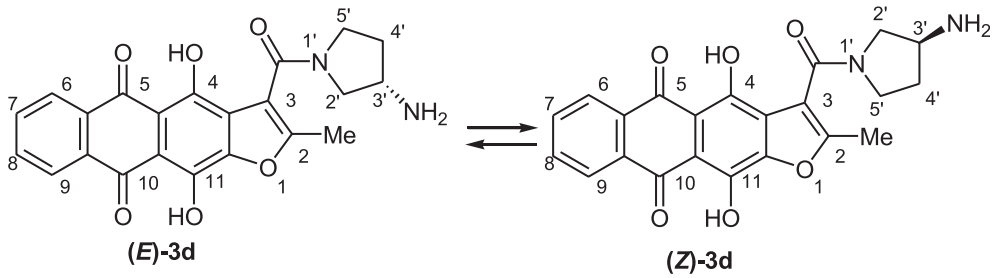

Scheme 3. Conversion of geometrical isomers (*E*/*Z*) of 4,11-dihydroxy-2-methyl-5,10-dioxoanthra [2,3-*b*]furan-3-carboxamide **3d**.

methyl-5,10-dioxoanthra[2,3-*b*]furan-3-carboxamides **3a**–**m** was tested against a panel of wild type cell lines and isogenic drug resistant sublines, that is, murine leukemia L1210, human cervical carcinoma HeLa, K562 myeloid leukemia and its multidrug resistant (MDR), P-glycoprotein (Pgp) expressing K562/4 variant, as well as human colon carcinoma HCT116 cell line and HCT116p53KO subline with genetically inactivated p53.

All new compounds (**3a**–**m**) inhibited tumor cell proliferation at submicromolar or low micromolar concentrations. The most potent was the derivative of (*S*)-3-aminopyrrolidine **3d** which inhibited the proliferation of wild tumor cell lines at submicromolar concentrations. Its antipode **3c** was slightly weaker against the majority of tested cell lines. Their regioisomers **3a**,**b** were less active against L1210 and Hela but more potent for colon carcinoma HCT116. The analogues **3f**–**k**,**m** with 3- aminopiperidine, 4-aminopiperidine, piperazine and 3-aminoquinuclidine residues in the side chains largely showed a lower potency than **3d** (Table 1). Their analogue with ternary amino group (*N*-methylpiperazine) in the side chain substantially (10–100 fold) decreased the antiproliferative potency of **3l** against almost all tested tumor cell lines.

The majority of new anthra[2,3-*b*]furan-3-carboxamides were cytotoxic for wild type cell lines as well as to their isogenic drug resistant counterparts. The K562/4 cells express functional Pgp and are resistant to the Pgp transported drug **1** (resistance indices RI ≈ 43, Table 1). In contrast, for anthra[2,3-*b*]furan-3-carboxamides **3a**–**h**,**m** and for naphtho[2,3-*f*]indole-5,10-dione **2** the resistance indices were close to or less than 1. The activity of **3e** and **3h** was even higher against Pgp-positive cells than for parental K562 counterparts (RI = 0.6 and 0.15, respectively; Table 1). Compounds **3a**, **c**–**j**, **m** exhibited a similar toxicity for the HCT116p53KO ($p53^{-/-}$) subline and the wild type HCT116 cell line (RI = 0.75 and 0.5, respectively) as opposed to a lower sensitivity of HCT116p53KO subline to doxorubicin (Dox) **1** (RI = 5.0; Table 1).

To evaluate the cytotoxicity of new agents for non-malignant cells we tested **3c** and **3d** against hFB-hTERT6 skin fibroblasts. Both compounds were virtually non-toxic (IC_{50} > 50 μM after a 72 h continuous cell exposure). Moreover, no detectable cytotoxicity of **3c** and **3d** was observed against donor peripheral blood lymphocytes (data not shown). These data further justified an in-depth investigation of the new perspective chemotype.

Overall, new anthra[2,3-*b*]furan-3-carboxamides demonstrated a high antiproliferative potency against tumor cells with two major determinants of altered drug response, namely, Pgp expression and p53 inactivation. Thus, scaffold hopping and subsequent optimization of the structure of the diamine moiety in the side chain of anthra[2,3-*b*]furan-3-carboxamides yielded candidates for an in-depth evaluation as drug candidates.

Table 1
Structure and antiproliferative activity (IC_{50}[a]) of 4,11-dihydroxy-2-methyl-5,10-dioxoanthra[2,3-*b*]furan-3-carboxamides **3a**–**m**.

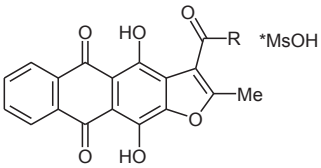

Cmpd	R	L1210	HeLa	K562	K562/4	RI[b]	HCT116	HCT116(−/−)	RI[c]
3a	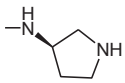	5.4 ± 2.3	9.5 ± 5.9	0.7 ± 0.1	0.75 ± 0.1	1.1	0.3 ± 0.02	0.2 ± 0.1	0.7
3b	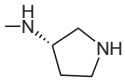	6.5 ± 1.2	64 ± 48	0.75 ± 0.1	0.8 ± 0.1	1.1	0.25 ± 0.04	0.5 ± 0.1	2
3c	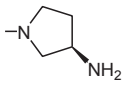	1.9 ± 1.6	2.1 ± 0.7	1.1 ± 0.15	1.3 ± 0.2	1.2	1.2 ± 0.2	1.3 ± 0.2	1.1
3d	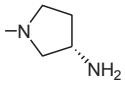	0.6 ± 0.1	0.5 ± 0.1	0.9 ± 0.1	1.4 ± 0.2	1.5	0.8 ± 0.2	0.8 ± 0.2	1
3e	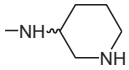	3.0 ± 0.2	3.4 ± 3.0	0.6 ± 0.1	0.35 ± 0.04	0.6	1.6 ± 0.2	1.6 ± 0.2	1
3f	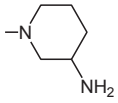	5.6 ± 1.8	1.4 ± 0.7	0.85 ± 0.1	0.7 ± 0.1	0.8	1.5 ± 0.2	1.6 ± 0.2	1.1
3g	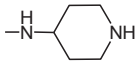	5.1 ± 0.2	11 ± 9	2.7 ± 0.3	4.0 ± 0.5	1.5	1.2 ± 0.1	0.7 ± 0.3	0.6
3h	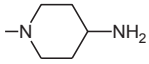	13 ± 10	9.7 ± 7.4	2.1 ± 0.2	0.4 ± 0.06	0.15	2.0 ± 0.2	2.1 ± 0.1	1
3i	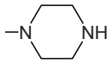	4.1 ± 0.0	3.1 ± 1.3	1.3 ± 0.17	2.8 ± 0.4	2.1	2.3 ± 0.3	2.2 ± 0.3	1.0
3j	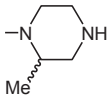	3.7 ± 0.3	0.7 ± 0.1	1.1 ± 0.14	4.8 ± 0.6	4.7	1.6 ± 0.2	1.3 ± 0.2	0.8
3k	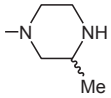	3.7 ± 0.7	0.9 ± 0.4	0.9 ± 0.1	3.0 ± 0.4	3.3	1.3 ± 0.1	3.7 ± 0.5	3.0
3l	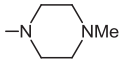	82 ± 38	104 ± 57	1.6 ± 0.2	5.9 ± 0.7	3.8	11.5 ± 2	25 ± 3	2.2
3m	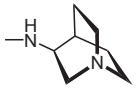	2.4 ± 0.7	12 ± 15	0.6 ± 0.08	0.65 ± 0.1	1.1	0.9 ± 0.1	0.8 ± 0.1	0.9
1	–	0.4 ± 0.1	nt[d]	0.1 ± 0.03	4.3 ± 0.52	43	0.1 ± 0.03	0.5 ± 0.1	5.0
2	–	0.07 ± 0.02	nt[d]	0.4 ± 0.1	0.4 ± 0.06	1.0	1.6 ± 0.4	1.2 ± 0.1	0.7

Compounds **1** and **2** were used as reference agents.
[a] IC_{50}, μM (mean ±S.D. of 3 experiments).
[b] RI, resistance index: IC_{50}(K562/4)/IC_{50}(K562).
[c] RI, resistance index: IC_{50}(HCT116p53KO)/IC_{50}(HCT116).
[d] Not tested.

2.2.2. Intracellular accumulation in wild type and Pgp-expressing cells

Based on the screening of the antiproliferative potency we selected **3c** and **3d**, the compounds differed only in the configuration of the NH_2-substituted carbon in the carboxamide ring. These stereoisomers were highly potent against parental and drug resistant tumor cells; however, **3d** was more active (Table 1). To address the question of whether Pgp efflux can be circumvented

by **3c** and **3d**, we analyzed the time course of intracellular accumulation of these agents in K562 and K562/4 cells. As shown in Fig. 3, the reference drug Dox (**1**) readily accumulated in K562 cells after 1 h; by 24 h of exposure the cell associated fluorescence increased significantly whereas the brightness of Pgp-positive K562/4 cells increased to a much lesser extent. In contrast, fluorescence of K562 and K562/4 cells loaded with **3c** or **3d** increased similarly over time (Fig. 3). These results suggested that **3c** or **3d** are weaker substrates for Pgp mediated transport than **1**, the drug used for selection of K562/4 subline. In other words, selection for survival in the presence of **1** conferred a Pgp mediated MDR phenotype but no cross-resistance to **3c** or **3d**.

2.2.3. Cell cycle distribution and apoptosis

Pgp is not the sole mechanism that can limit the cytotoxicity of anthraquinone derivatives. As shown in Table 1, HCT116p53KO cells with genetically inactivated pro-apoptotic p53 were resistant to **1** (RI = 5.0). Advantageously for the new chemotype, the majority of compounds listed in Table 1 were similarly or even preferentially toxic for HCT116p53KO subline than for wild type HCT116 cells. The exceptions were **3b**, **3k** and **3l** (RI $\geq$ 2); still, **3b** and **3k** were potent at submicromolar or low micromolar concentrations (Table 1). To address the question of whether our new compounds can alter cell cycle distribution and cause cell death, we treated HCT116 and HCT116p53KO cells with **3c** or **3d** at 1 μM, a concentration comparable to IC_{50}. After 24 h of cell exposure the percentage of events in G2/M phase increased statistically; this effect was paralleled by an increase of subG1 values and a concomitant decrease of G1 and S (Fig. 4). The most noticeable changes were detectable by 48 h. The majority of cells underwent late stages of apoptosis as determined by the predominance (>70%) of events in subG1. Thus, the arrest in G2/M preceded DNA fragmentation. Importantly, the time course of these changes was similar in HCT116 and HCT116p53KO cells; therefore, the lack of functional p53 did not rescue cells, nor did it change the sequence of death associated events, that is, G2/M block followed by DNA degradation (Fig. 4). Treatment of HCT116 and HCT116p53KO cells with 1 μM **3c** resulted in essentially the same time course of cell cycle changes as treatment with **3d** (not shown).

Furthermore, staining with Annexin V-FITC and PI of HCT116 and HCT116p53KO cells exposed to 1 μM **3d** showed an increased percentage of apoptotic (Annexin V^+/PI^-) events by 24 h (Table S1). The portion of PI^+ (late apoptotic or necrotic) cells also increased statistically although to a lesser degree. By 48 h we observed a significant elevation of both Annexin V^+/PI^- and Annexin V^+/PI^+ events, indicating that apoptosis was the predominant mode of cell death. Importantly, as for cell cycle distribution, no substantial difference of respective parameters was detected between HCT116 and HCT116p53KO cells (Table S1). Compound **3c** caused similar changes of Annexin V and PI reactivity in both cell lines (not shown).

Thus, **3c** and **3d** emerged as new potent cytotoxic agents for a variety of mammalian tumor cell lines including those with molecular determinants of altered drug response, i.e., Pgp expression or p53 inactivation. These compounds induced apoptosis preceded by, or concomitant with, G2/M arrest. Considering their perspective as drug candidates, we examined **3c** and **3d** for their ability to interact with tentative intracellular targets such as DNA and protein kinases, interfere with Top1 and 2 function, and to prolong the life span of tumor bearing mice.

2.3. Interaction with intracellular targets

2.3.1. Complexes with duplex DNA

Intercalation into the DNA and/or the formation of ternary complexes between the drug, DNA and topoisomerases are the key prerequisites of antitumor activity of anthracyclines and their derivatives [19]. The spectrophotometric analysis of interaction of **3c** and **3d** with DNA isolated from calf thymus (ctDNA) showed a decreased (~36%) extinction of the absorption maxima at 483 nm and a 9 nm bathochromic shift upon the increase of ctDNA concentration, reflecting the formation of complexes between each compound and the duplex DNA (Fig. 5A, C).

Significant changes in fluorescence spectra of **3c** and **3d** in complexes with DNA were observed. Similarly to **1**, the increase of DNA concentration led to almost complete quenching of fluorescence of **3c** and **3d** (Fig. 5B, D). These changes can be explained by intercalation of the chromophores between DNA base pairs. Furthermore, DNA-ligand complex formation resulted in a substantially decreased polarity of the medium and the emergence of stacking interactions between the anthraquinone nucleus and DNA base pairs.

To build the binding isotherms, the concentration of bound (C_b) and free (C_f) compounds were determined by changes of absorption (ε) at 470 nm using the formulas:

$$C_b = (\varepsilon - \varepsilon_f)/(\varepsilon_b - \varepsilon_f);\ C_f = C_0 - C_b$$

where C_0 is the concentration of compound in solution, ε_b and ε_f are the extinction of bound and free drug.

Average DNA fill is the ratio of bound compound to one DNA base pair ($r = C_b/C_{DNA}$). Using the found concentrations the binding isotherms were generated in Scatchard coordinates (Fig. 6). The binding constant (K_a) was determined by approximating experimental isotherms with McGhee-von Hippel equation [20]:

$$\frac{r}{C_f} = K_a(1 - n\cdot r)\left(\frac{1 - n\cdot r}{1 - (n-1)\cdot r}\right)^{(n-1)},$$

where K_a is the binding constant, r is the average number of bound ligand molecules per one base pair ($r = C_b/C_{DNA}$), n is the number of

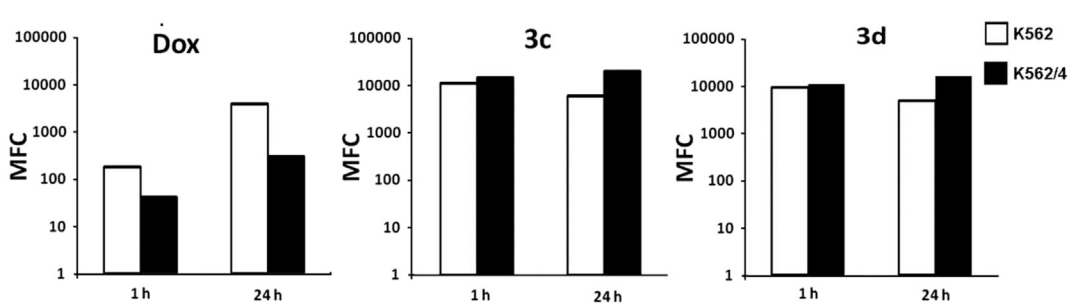

Fig. 3. Intracellular accumulation of **3c** and **3d** in K562 and K562/4 cells. Cells were treated with 1 μM of **Dox**, **3c** or **3d** for indicated time intervals, washed with ice cold saline and immediately analyzed by flow cytometry. Shown are data of one representative experiment out of total three with essentially the same results.

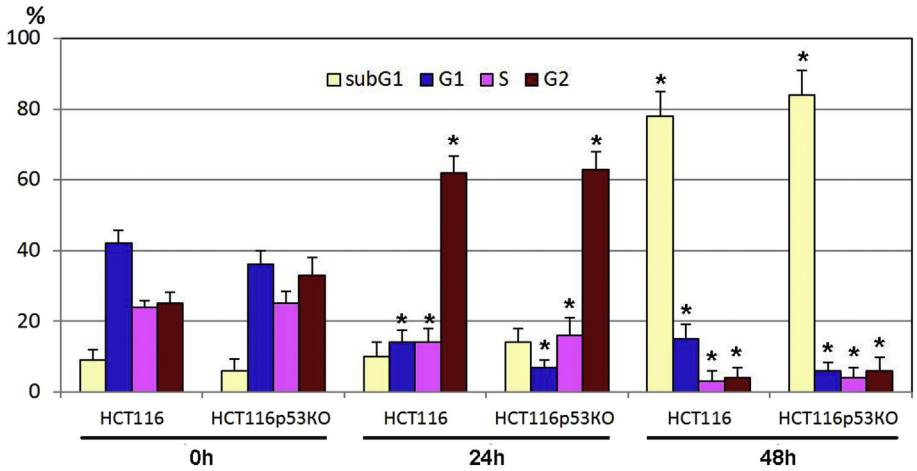

Fig. 4. Cell cycle distribution in HCT116 and HCT116p53KO cells treated with **3d**. Values are % events. *$p < 0.05$ between drug treated and untreated (0 h) groups. Data are mean ± SD of four independent experiments.

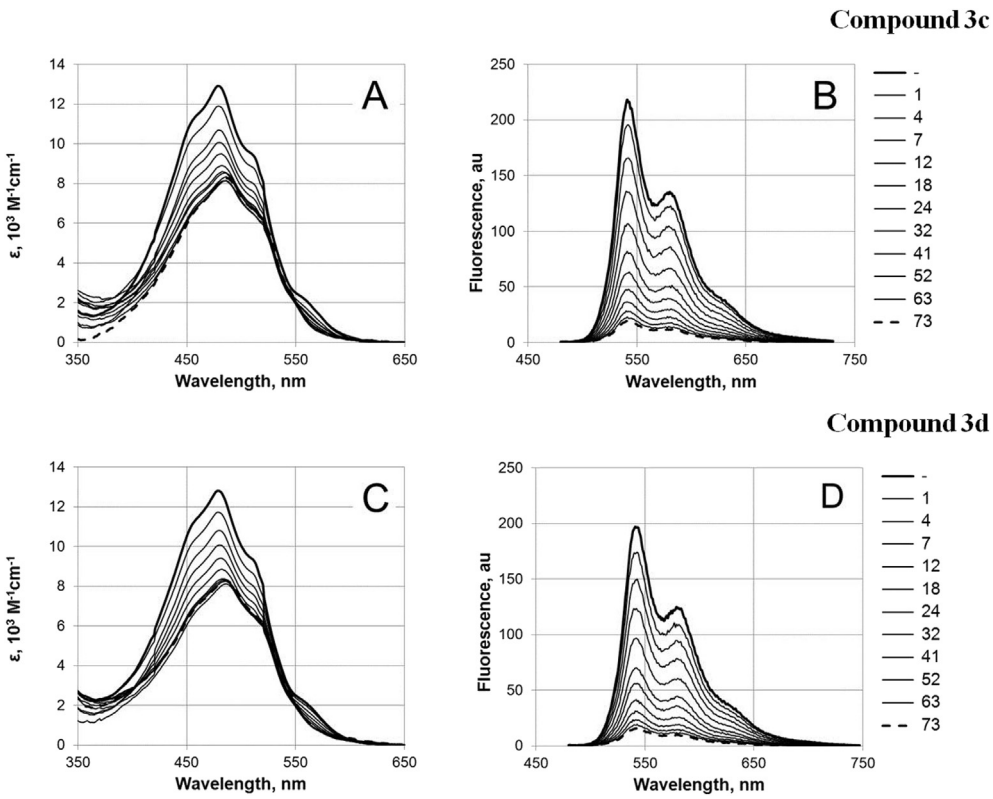

Fig. 5. Changes in absorbance (A, C) and fluorescence (B, D) spectra of **3c** and **3d** depending on DNA concentration. Concentrations: **3c** and **3d** 5 μM; ctDNA concentrations (μM, base pairs) are indicated to the right.

base pairs bound to one molecule of the ligand (exclusion length).

The dissociation constants *KD* were calculated as reciprocal of *Ka*. The determined binding constant (*Ka*) parameters of drug-duplex interaction are presented in Table 2.

Both **3c** and its stereoisomer **3d** formed stable complexes with ctDNA at micromolar concentrations. Compound **3d** demonstrated a slightly greater affinity to DNA than **3c**, but for both stereoisomers the binding constants (*Ka*) were 2–3-fold smaller than for reference compounds **1** [21] or **2** [12].

To elucidate the mode of interaction with DNA, **3c** and **3d** were docked to the duplex (PDB: 2DES) using Molsoft ICM version 3.8. Because NMR studies suggested a dynamic mixture of *E*/*Z* isomers of the amide bond, for molecular modeling two *E*/*Z* isomers of **3c** and **3d** were used. Fig. 7 shows that the binding modes of *E*/*Z* isomers for **3c** and **3d** were similar to **1** (complexes of **1** with DNA are known from crystallographic data) [22]. Similarly to **1**, compounds **3c** and **3d** were anchored within the minor groove of the duplex [23]. The chromophores intercalated between base pairs G(1)-C(12) and C(2)-G(11) (intercalation site). The central moiety of the intercalated chromophore was engaged in extensive stacking interactions with flanking base pairs. This led to the formation of hydrogen bonds between the ligands' hydroxyl groups and O atoms

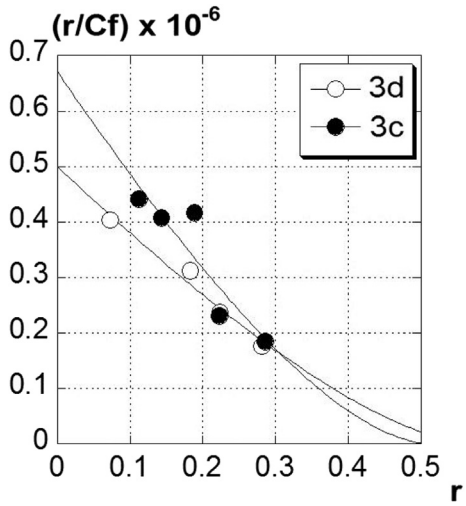

Fig. 6. Binding isotherms of **3c** and **3d** with ctDNA shown as Scatchard plot. Solid curves are the theoretical fit with McGhee-von Hippel equation.

Table 2
Binding parameters of **3c** and **3d** with duplex DNA.

Compound	K_a, M^{-1}	K_D, μM	L, bp
3c	$5.0 \pm 0.5 \times 10^5$	2.0 ± 0.2	1.7 ± 0.2
3d	$6.7 \pm 1.0 \times 10^5$	1.5 ± 0.2	1.9 ± 0.3

of the furanose rings of the duplex backbone, thereby significantly stabilizing the complexes. The furan cycle with the side diamine residues (localized to the minor groove) further stabilized the complexes by van der Waals and Coulomb's interactions between the terminal amino group and the phosphate groups of A(3)-T(10) at the distance 3.8–4.7 Å. Additionally, like the amino group of the daunosamine residue of **1** [23], in the complexes of (*E*)-**3c** and (*E*)-**3d** with DNA the terminal amino groups of the ligands interacted with 'backside' carbonyl group of T(10) of the pair next to the intercalation site (NH … O distance 2.1–2.3 Å). Thus, in general, the obtained structures of complexes of **3c** and **3d** with the DNA duplex are similar, just slightly depending on geometry of 3-aminopyrrolidine residue in the side chain of ligands. The calculation of free binding energy (Table S2) showed similar results of (*E*)-**3c** and (*E*)-, (*Z*)-**3d** ($\Delta G_{sum} \sim -5.6$ kcal/mol) whereas (*Z*)-**3c** formed somewhat less stable complexes ($\Delta G_{sum} = -5.0$ kcal/mol). The docking results are in concert with experimental data that showed a higher affinity of **3d** than of **3c** to ctDNA (Table 2). Also, the molecular modeling confirmed that binding to DNA of anthrafuran-3-carboxamides can alter the structure of the duplex, the fact important for understanding the mechanisms of antitumor effects of these compounds (see below).

2.3.2. Top1 and Top2 inhibition

Given that **3c** and **3d** are DNA binders, we investigated the ability of these compounds to interfere with DNA modifying enzymes Top1 and 2. Fig. 8A shows that both compounds attenuated Top1 mediated relaxation of the supercoiled plasmid DNA in a dose

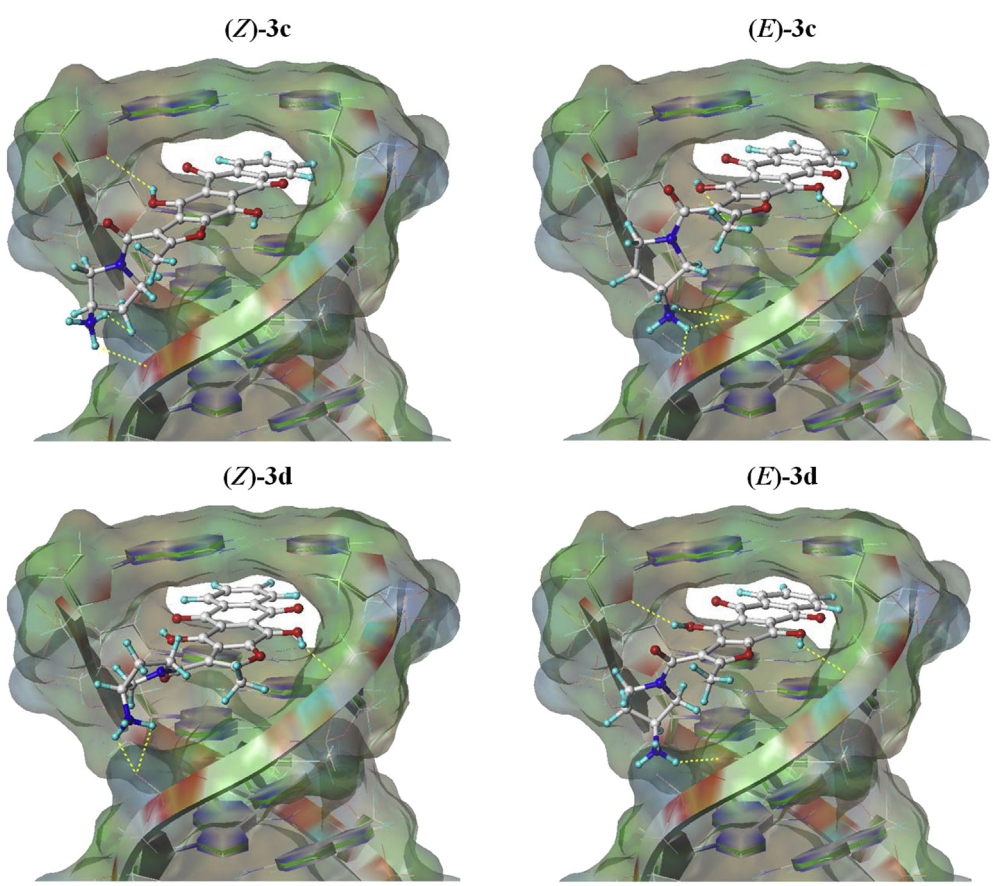

Fig. 7. Docking of *E*– and *Z*-conformers of **3c** and **3d** into duplex DNA (ICM; PDB: 2DES). Hydrogen bonds are shown in yellow. The solvent-accessible Conolly surface of the duplex was colored depending on hydrophobicity potential. (For interpretation of the references to colour in this figure legend, the reader is referred to the web version of this article.)

dependent manner. At concentrations ≤1 μM neither compound influenced the ability of the enzyme to generate slowly migrating DNA topoisomers whereas at 5 μM and 10 μM one can observe faster migrating DNA molecules. Next, we tested whether **3c** and **3d** induce specific DNA clevage, a mechanism known for Top1 poisons camptothecin (CPT) and indenoisoquinoline MJ–III–65 (NSC 706744) [24]. Incubation of Top1 with an oligonucleotide carrying Top1 cleavage sites [25] in the presence of CPT or MJ–III–65 resulted in a pattern of bands characteristic for specific Top1 poisons (Fig. 8B). Compound **2** cleaved some but not all these sites. In contrast, **3c** or **3d** poorly generated the specific DNA cleavage, suggesting that Top1 inhibition by **3c** and **3d** is not associated with the drug-DNA-enzyme complex formation.

Furthermore, **3c** and **3d** were similarly potent as Top2 blockers although this enzyme was attenuated to a lesser extent: even at 40 μM a certain amount of relaxed plasmid DNA was detectable (Fig. 8C, *bottom panel*). In this assay etoposide (VP16) was significantly less potent than **3c** or **3d**: even at 200 μM of VP16 the DNA remained largely unwound. Thus, a dual Top1/2 inhibitory activity was attributed to the newly synthesized chemotype.

2.3.3. Modulation of protein kinase activity

Protein kinases, the key regulators of a plethora of important processes including cell survival in response to chemotherapeutic drugs [26], can be targets for hydroxyanthraquinones [27–29]. In *in vitro* kinase assays our new heterocyclic anthraquinone derivative **3d** attenuated only nine out of 364 (2.5%) human protein kinases (screened by ProQinase GMBH; Freiburg, Germany) at micromolar concentrations (IC_{50} < 5 μM), suggesting a reasonable enzyme selectivity. Among down-regulated enzymes were serine/threonine protein kinases Aurora B and C, kinases of mitogen activated cascades MKNK1 and MAP3K7/MAP3K7IP1, pro-proliferative/anti-apoptotic Pim1 and -3, nuclear receptor kinases RIPK5, TLK1 and the tyrosine kinase of fibroblast growth factor receptor with missense mutation FGF-R1 (V561M) (Fig. 9). These enzymes are mechanistically involved in regulation of cell division and survival. Although none of the above protein kinases was completely inhibited by tested concentrations of **3d**, the multiplicity of attenuated targets can be important for antitumor properties of this compound.

Attenuation of protein kinase activity was illustrated by simulation of **3d** binding to Aurora B (PDB: 4A3F) using Molsoft ICM. Both *E*- and *Z*- conformers of this compound fit well to the ATP

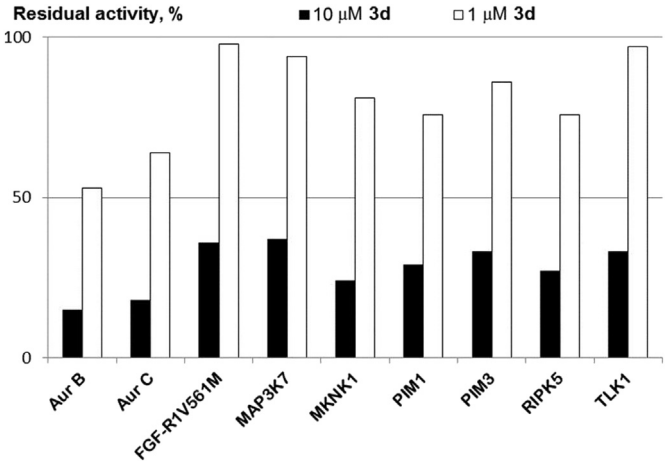

Fig. 9. Attenuation of *in vitro* protein kinase activity by **3d**. Values are percent activity of the respective enzyme incubated in the presence of 1 μM or 10 μM **3d**. The enzyme activity in the absence of **3d** was taken as 100%. Shown are data of one out of 3 experiments with similar results. Aur B, Aur C: Aurora B or Aurora C protein kinase, respectively.

binding site of the enzyme (Fig. 10A, B). The complexes were significantly stabilized by strong hydrophobic interactions (see ΔG_{surf} value in Table S2) as the anthraquinone fragment of **3d** completely immersed into the hydrophobic cavity of the ATP binding cleft (Fig. 10A, B, S3, S4). Additionally, the complexes can be stabilized by hydrogen bonds between the functional groups of **3d** and the amino acid residues that form the ATP binding site (Figs. 10A, B, S4). It should be noted that the complex of *Z*-isomer with Aurora B was substantially more stable than the complex formed by *E*-isomer ($\Delta G_{sum} = -4.49$ *vs* -3.88 kcal/mol, Table S3).

For both *E*- and *Z*-conformations of **3d** the carbonyl and hydroxyl groups of the chromophore in positions 10 and 11 formed a hydrogen bond with the elements of peptide bonds of Ala157 and Pro158 (Figs. S4 A,B). For *Z*-conformation of **3d** a significant contribution into the complex stabilization was provided by hydrogen bonds between the amino group of the pyrrolidine moiety and the functional groups in Gly84 and Glu161, and by the ionic interaction with carboxylic group of Glu161 (Fig. 10B, S4). The complex can be further stabilized by a hydrogen bond between the carbonyl group of the carboxamide moiety in **3d** and NH groups in

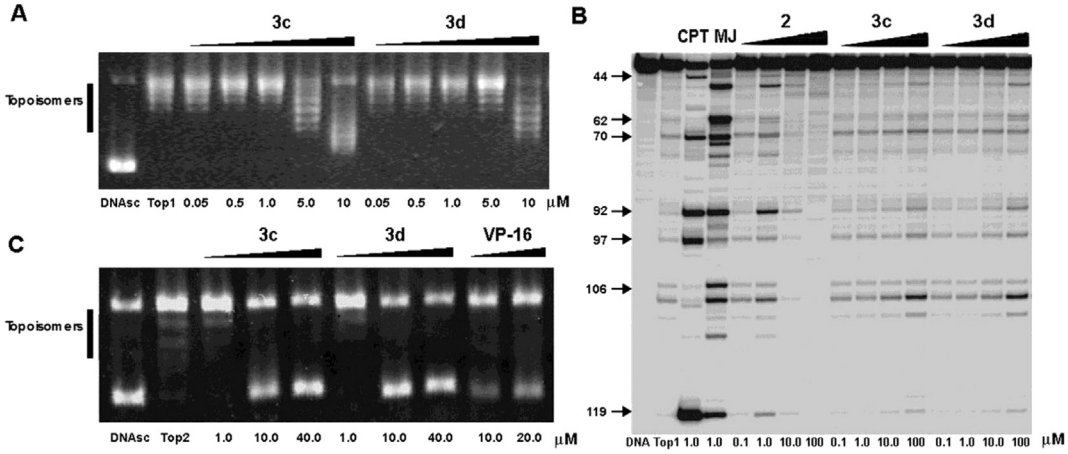

Fig. 8. Effects of **3c** and **3d** on Top1 and Top2 function. Attenuation of Top1 (**A**) and Top2 (**C**) mediated plasmid DNA relaxation. DNAsc, supercoiled plasmid conformation. **B**, Top1 mediated DNA cleavage by **3c** and **3d** and naphthoindoledione **2**. Lanes: 1, DNA alone; 2, + Top1; 3, + **CPT** 1 μM; 4, + **MJ-III-65**, 1 μM; lanes 5–16, + **2**, **3c** and **3d** at indicated concentrations (μM). Numbers on the left and arrows indicate cleavage site positions [25].

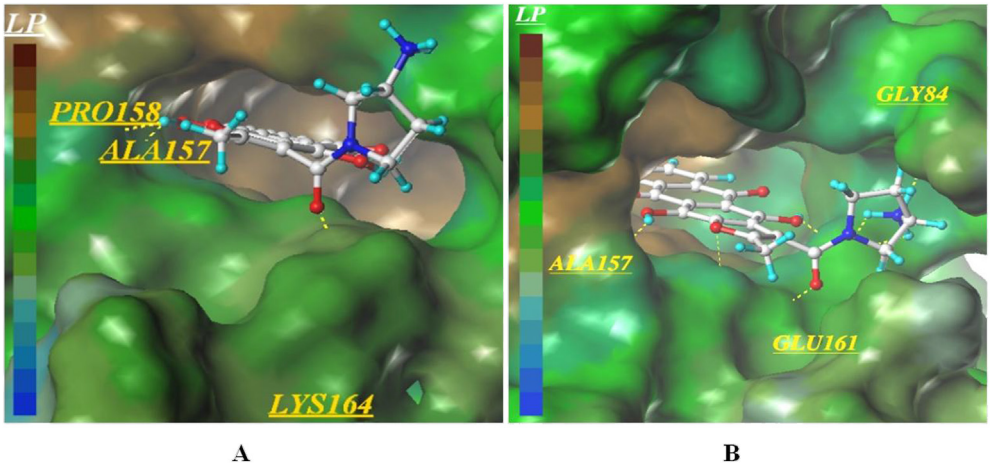

Fig. 10. Molecular docking of *E*-(A) and *Z*-(B) isomers of **3d** into Aurora B (ICM; PDB: 4A3F). The solvent-accessible Conolly surfaces of the enzyme are colored depending on hydrophobic potential. (For interpretation of the references to colour in this figure legend, the reader is referred to the web version of this article.)

Lys164 or Glu161 located outside of the ATP binding pocket (Fig. 10A, B, S3, S4). Thus, the docking model of binding to Aurora B identified the role of individual structural fragments of **3d**, especially the importance of the carboxamide moiety and the stereochemistry of the diamine residue. In contrast, the parental naphthoindoledione **2** and its regio- and stereoisomers with the methylene spacer were much weaker inhibitors of Aurora B *in vitro* (IC_{50} = 130–150 μM), further highlighting a critical role of the carboxamide group in targeting protein kinases by **3d**.

Thus, compound **3d** is capable of interacting with different biomacromolecules. This multiplicity is not surprising since structurally close anthraquinone derivatives with modified side chains have been reported to bind not only to the duplex DNA but to the complex DNA structures such as guanine quadruplexes [9,10]. The ability to bind to a variety of important targets, thereby triggering several death pathways, should be an advantageous property for the drug candidate.

2.3.4. Antitumor activity in vivo

We tested the antitumor efficacy of stereoisomers **3c** and **3d** in a model of i.p. transplanted P388 leukemia as a percent mean life span (MLS) in treated (T) *vs* untreated (control, C) groups, T/C. As minimal criterion of therapeutic efficiency T/C ≥ 125% was used. MLS in the untrated group was taken as T/C = 100%. These assays allowed for comparison of therapeutic potencies of new compounds with our previous series of naphthoindolediones [12]. As shown in Table 3, the effect of **3c** at the single dose of 30 mg/kg daily for 5 days (total dose 150 mg/kg) was close to minimal criterion of therapeutic efficiency T/C = 122% (MLS = 11.8 ± 1.1 days) while in the untreated group MLS was 9.7 ± 1.1 days. Only with the single tolerated dose of 50 mg/kg (total 250 mg/kg) we achieved T/C = 178% ($p < 0.05$). In striking contrast, the stereoisomer **3d** at the single tolerated dose of 30 mg/kg (total 150 mg/kg) showed a more pronounced antitumor efficacy (T/C = 214%; $p < 0.05$). At the single dose of 50 mg/kg (total 250 mg/kg) **3d** was lethally toxic (Table 5), with the spleen mass decreased down to 40% (average 87 mg *vs* 142 mg in the control group). Thus, in the 5 days daily regimen **3d** (at the tolerated dose) was more potent than **3c**.

A detailed dose response revealed a higher antitumor efficacy of **3d** injected i.p. with single doses of 5–40 mg/kg daily for 5 days (total 25–200 mg/kg). Table 4 shows that **3d** with at all tested doses significantly prolonged the life span of mice bearing i.p. translanted P388 tumor: T/C = 140–262% ($p < 0.05$). No signs of general drug toxicity were registered during or after treatment.

Table 3
Antitumor efficacy of **3c** and **3d** against murine i.p. transplaned P388 leukemia.

Group[a]	Dose, mg/kg[b]		MLS[c], days	T/C, %
	Single	Total		
Control, saline	NA[d]	NA	9.7 ± 1.1	100
3c	30	150	11.8 ± 1.1	122
	50	250	17.3 ± 0.9	178
3d	30	150	20.8 ± 1.2	214
	50	250	6.5 ± 1.3	death from drug toxicity

[a] n = 6.
[b] Drugs were administered i.p. daily on days 1–5 after i.p. transplantation of P388 leukemia cells.
[c] Mean ± S.D.
[d] NA, not applicable.

Thus, the strongest antitumor efficacy of **3d** was achieved with the single dose of 30–40 mg/kg daily for 5 days (total 150–200 mg/kg; T/C up to 262%). Also, a reasonable effect could be accomplished with 20 mg/kg daily (total 100 mg/kg), a well tolerated dose that increased MLS more than twofold. The therapeutic perspective of **3d** can be further proved by its advantage over the prototype naphtho[2,3-*f*]indole-5,10-dione **2** in a similar treatment schedule (T/C_{max} = 155%, total dose 150 mg/kg for five days [12]).

3. Conclusion

We applied the 'scaffold hopping' approach to obtain a new chemotype, that is, anthra[2,3-*b*]furan-3-carboxamides as

Table 4
Life span of mice with i.p. P388 leukemia transplants.

Group[a]	Dose, mg/kg[b]		MLS[c], days	T/C, %
	Single	Total		
Control (saline)	NA[c]	NA[c]	9.6 ± 0.5	100[c]
3d	5	25	13.4 ± 0.4	140[d]
	10	50	16.3 ± 0.1	170[d]
	20	100	21.3 ± 1.2	222[d]
	30	150	24.9 ± 2.1	260[d]
	40	200	25.2 ± 4.3	262[d]

[a] n = 11.
[b] i.p. injections daily on days 1–5 after inoculation of P388 leukemia cells.
[c] NA, not applicable.
[d] $p < 0.05$. Averaged data of four experiments.

perspective antitumor compounds. Our hypothesis was founded on the known anticancer efficacy of the anthraquinone scaffold present in conventional chemotherapeutic drugs such as **1** and its derivatives. Modifications of the anthraquinone scaffold, in particular, hetarene fused anthracenediones, have yielded the agents with improved properties [8–12]. In this report we for the first time synthesized a series of potently antiproliferative anthra[2,3-*b*]furan-3-carboxamides and selected two stereoisomers, **3c** and **3d**, for mechanistic studies. Unlike **1**, compounds **3c** and **3d** were similarly cytotoxic against wild type tumor cells of different tissue and species origin, and to their isogenic sublines with the determinants of altered drug response such as Pgp or non-functional p53. Both stereoisomers formed stable complexes with the duplex DNA and attenuated the DNA dependent enzymes Top1 and Top2 *in vitro*. Interestingly, the mechanism of Top1 attenuation by **3c** and **3d** was fundamentally different from that displayed by reference agents CPT or MJ–III–65 known to entrap tertiary drug-DNA-enzyme complexes. Our models of interaction of **3c** and **3d** with DNA suggest an interfacial mode of Top1 inhibition [30]. In contrast, compound **2** can be regarded as a more specific Top1 inhibitor [12]; therefore, scaffold hopping can generate structurally close compounds with substantially different mechanisms and properties. Along with a lower specificity of Top1 inhibition, compound **2** at 1 μM attenuated this enzyme more potently than compounds **3c** and **3d** at 10 μM ([12] and this study).

The ability of **3d** to down-regulate a set of human protein kinases *in vitro*, as well as the virtual models of interaction of **3c** and **3d** with Aurora B, add protein kinases to the growing list of intracellular targets important for antitumor properties of heteroaren-fused anthracendeiones. Recently we demonstrated that our chloroacetamidine derivatives of anthrathiophenedione can bind not only to the duplex DNA but to guanine quadruplexes, implicating G-quadruplex carrying regulatory regions in the *H-Ras* oncogene as a target [9]. We consider the multiplicity of biomacromolecules 'druggable' by different heteroaren-fused anthracenediones as a therapeutic advantage since a variety of death signaling pathways would be engaged. It could be that, regardless of a certain lack of specificity to target or a lesser value of individual parameters (such as DNA binding constant or intracellular accumulation in case of several anthra[2,3-*b*]thiophene-5,10-diones [31]), a compound with reasonable *in vivo* therapeutic efficacy and tolerance can be obtained.

Indeed, the scaffold hopping produced a practically valuable 'property hopping' that led to the discovery of the potent antitumor anthra[2,3-*b*]furan-3-carboxamides available for large-scale preparation. Compound **3d** was efficient against the murine intraperitoneally transplanted P388 leukemia (an increase of animals' life span up to 262%). The stereoisomer **3c** was less potent in cell culture and *in vivo*. Further in-depth development of this novel class is expected to yield next generations of synthetic anthracycline analogues with improved therapeutic properties.

4. Experimental section

4.1. General methods

NMR spectra of all newly synthesized compounds were recorded on a Varian VXR-400 instrument at 400 MHz (^{1}H NMR) and 100 MHz (^{13}C NMR). Chemical shifts were measured in DMSO-d_6 or $CDCl_3$ using TMS as an internal standard. Analytical TLC was performed on silica gel F254 plates (Merck) and column chromatography on Silica Gel Merck 60. Melting points were determined on a Buchi SMP-20 apparatus and are uncorrected. High resolution mass spectra were recorded by electron spray ionization on a Bruker Daltonics microOTOF-QII instrument. UV spectra were recorded on a Hitachi-U2000 spectrophotometer. HPLC was performed using Shimadzu Class-VP V6.12SP1 system (GraseSmart RP-18, 6 × 250 mm). Eluents: A, H_3PO_4 (0.01 M); B, MeCN. All solutions were evaporated at a reduced pressure on a Buchi-R200 rotary evaporator at temperature below 50 °C. All products were dried under vacuum at room temperature. All solvents, chemicals, and reagents were obtained from Sigma-Aldrich (unless specified otherwise) and used without purification. The naphtho[2,3-*f*]indole-5,10-dione **2** was prepared as described [12]. The purity of compounds **5**, **6**, **3a**–**m** was >95% as determined by HPLC analysis.

4.1.1. tert-Butyl 4,11-dihydroxy-2-methyl-5,10-dioxo-5,10-dihydroanthra [2,3-b]furan-3-carboxylate (5b)

To a stirring mixture of 2,3-dibromoquinizarin **4b** [15] (6.4 g, 16 mmol) and *tert*-butyl acetoacetate (9.0 ml, 54 mmol) in dimethyl sulfoxide (120 ml) the anhydrous potassium carbonate (7.0 g, 50 mmol) was carefully added at 120 °C. The mixture was stirred for 15 min to 125 °C, cooled and poured into vigorously stirred mixture of water (400 ml) and concd HCl (9 ml). The dark-brown precipitate was filtered, washed with water and ethanol (30 ml), and dried. The residue was purified by flash chromatography using hot (boiling) eluting solvent (toluene-chlorobenzene-ethyl acetate mixture, 3:1:1). The product was crystallized from chlorobenzene to give 62% yield of compound **5b** (4.4 g) as a red solid, mp 209–210 °C. HPLC (LW = 260 nm, gradient B 70 → 95% (20 min)) t_R = 25.43 min, purity 98.6%. $\lambda_{max.}$, EtOH (lgε): 260 (4.4), 449(4.0), 509 (3.9) nm. ν_{max}: 1715, 1622, 1611, 1585, 1453, 1424, 1363, 1325, 1307, 1277, 1167, 1128, 1082, 1024, 974 cm^{-1}. ^{1}H NMR (400 MHz, DMSO-d_6) δ 14.53 (1H, s, OH); 13.87 (1H, s, OH); 8.37 (2H, m, H-6,7); 7.81 (2H, m, H-8,9); 2.75 (3H, s, Me); 1.65 (9H, s, OBu^t). HRMS (ESI) calculated for $C_{22}H_{19}O_7$ [M+H]$^+$ 359.1125, found 395.1133.

4.1.2. 4,11-Dihydroxy-2-methyl-5,10-dioxo-5,10-dihydroanthra [2,3-b]furan-3-carboxylic acid (6)

To a stirring solution of anthrafurandione **5b** (4.0 g, 10 mmol) in hot chloroform (100 ml) trifluoroacetic acid (15 ml) was added. The mixture was stirred for 2 h and evaporated. Dichloromethane (50 ml) was added to the residue, the mixture was stirred 5 min and cooled. The precipitate was filtered, washed with dichloromethane (20 ml) and dried at 90 °C. Red crystals, yield 3.3 g (96%), mp 330–332 °C (mp 299–301 °C [14]). HPLC (LW = 260 nm, gradient B 70 → 95% (30 min)) t_R = 8.2 min, purity 99.0%. $\lambda_{max.}$, EtOH (lgε): 259 (4.4), 481 nm (4.0). ν_{max}: 1792, 1739, 1683, 1650, 1584, 1568, 1454, 1348, 1308, 1251, 1226, 1209,1156, 1126, 1016, 974 cm^{-1}. ^{1}H NMR (400 MHz, DMSO-d_6) δ 8.19 (2H, m, H-6,7); 7.91 (2H, m, H-8,9); 2.69 (3H, s, Me). HRMS (ESI) calculated for $C_{18}H_{11}O_7$ [M+H]$^+$ 339.0499, found 339.0504.

4.1.3. 4,11-Dihydroxy-2-methyl-5,10-dioxo-5,10-dihydroanthra [2,3-b]furan-3-carbonyl chloride (7)

A mixture of acid **6** (0.5 g, 1.5 mmol) and thionyl chloride (0.6 ml, 8.5 mmol) in benzene (50 ml) was vigorously stirred for 1 h and cooled. The resulting solution was evaporated under vacuum. The solid residue can be used at the next steps without purification. For analytical purposes the crude product was recrystallized from anhydrous benzene to afford 82% of acyl chloride **6** as a red powder with mp 212–213 °C. ^{1}H NMR (400 MHz, $CDCl_3$) δ 14.43 (1H, s, OH); 13.73 (1H, s, OH); 8.41 (2H, m, H-6,7); 7.86 (2H, m, H-8,9); 2.88 (3H, s, Me).

4.1.4. (R)-4,11-Dihydroxy-2-methyl-5,10-dioxo-N-(pyrrolidin-3-yl)-5,10-dihydroanthra [2,3-b]furan-3-carboxamide methanesulfonate (3a)

To a stirring mixture of crude acyl chloride **7** (prepared from acid **6** (500 mg, 1.5 mmol)) in anhydrous chloroform (30 ml) a

solution of (*R*)-1-Boc-3-aminopyrrolidine (600 mg, 3.4 mmol) and pyridine (0.6 ml, 7.0 mmol) in anhydrous chloroform (10 ml) was added. The mixture was refluxed for 5 min, diluted with chloroform (20 ml), washed with aqueous solution of HCl (0.3 M), dried and evaporated. The residue was purified by column chromatography on a silica gel in chloroform–methanol (10:0 → 10:1). The red solid obtained after evaporation was dissolved in hot chloroform (30 ml). Methanesulfonic acid (0.3 ml, 4.6 mmol) was added, the mixture was stirred overnight and evaporated. The residue was dissolved in boiling water (5 ml), filtered, the product was precipitated with acetone-ether mixture (3:1). The red solid was collected by filtration, washed with acetone, Et_2O, *n*-hexane and dried. The yield of methanesulfonate **3a** was 505 mg (71%) as a red solid, mp 333–335 °C (dec.). HPLC (LW = 260 nm, gradient B 20 → 60% (30 min)) t_R = 20.4 min, purity 97.2%. $\lambda_{max.}$, EtOH (lgε): 261 (4.4), 480 nm (4.0).ν_{max}: 1651, 1618, 1586, 1457, 1418, 1341, 1301, 1226, 1158, 1038 cm^{-1}. ^1H NMR (400 MHz, DMSO-d_6, 23 °C) δ 14.40 (1H, s, OH); 13.56 (1H, s, OH); 8.84 (3H, br. s, NH, NH_2); 8.15 (2H, m, H-6,7); 7.90 (2H, m, H-8,9); 4.53 (1H, m, NCH); 3.53 (1H, m, NCH_2); 3.32 (2H, m, NCH_2); 3.18 (1H, m, NCH_2); 2.64 (3H, s, Me); 2.34 (3H, s, SMe); 2.25 (1H, m, CH_2CH_2CH); 2.01 (1H, m, CH_2CH_2CH). HRMS (ESI) calculated for $C_{22}H_{19}N_2O_6$ $[M+H]^+$ 407.1238, found 407.1224. Analysis calculated for $C_{22}H_{18}N_2O_6{}^*CH_4O_3S{}^*2H_2O$, %: C 51.30, H 4.87, N 5.20. Found, %: 51.45, H 4.75, N 5.10.

4.1.5. (S)-4,11-Dihydroxy-2-methyl-5,10-dioxo-N-(pyrrolidin-3-yl)-5,10-dihydroanthra [2,3-b]furan-3-carboxamide methanesulfonate (**3b**)

This compound was prepared from **6** and (*S*)-1-Boc-3-aminopyrrolidine as described for **3a**. A red powder, yield 69%, mp 333–335 °C (dec.). HPLC (LW = 260 nm, gradient B 20 → 60% (30 min)) t_R = 20.5 min, purity 98.8%. $\lambda_{max.}$, EtOH (lgε): 261 (4.4), 480 nm (4.0). ν_{max}: 1651, 1618, 1586, 1457, 1418, 1341, 1301, 1226, 1158, 1038 cm^{-1}. ^1H NMR (400 MHz, DMSO-d_6, 23 °C) δ 14.38 (1H, s, OH); 13.55 (1H, s, OH); 8.84 (3H, br. s, NH, NH_2); 8.15 (2H, m, H-6,7); 7.90 (2H, m, H-8,9); 4.53 (1H, m, NCH); 3.53 (1H, m, NCH_2); 3.32 (2H, m, NCH_2); 3.18 (1H, m, NCH_2); 2.64 (3H, s, Me); 2.34 (3H, s, SMe); 2.25 (1H, m, CH_2CH_2CH); 2.01 (1H, m, CH_2CH_2CH). HRMS (ESI) calculated for $C_{22}H_{19}N_2O_6$ $[M+H]^+$ 407.1238, found 407.1224. Analysis calculated for $C_{22}H_{18}N_2O_6{}^*CH_4O_3S{}^*2H_2O$, %: C 51.30, H 4.87, N 5.20. Found, %: 51.45, H 4.75, N 5.10.

4.1.6. (R)-3-(3-Aminopyrrolidine-1-carbonyl)-4,11-dihydroxy-2-methylanthra [2,3-b]furan-5,10-dione methanesulfonate (**3c**)

This compound was prepared from **6** and (*R*)-3-(Boc-amino) pyrrolidine as described for **3a**. An orange-reddish powder, yield 75%, mp 327–328 °C (dec.). HPLC (LW = 260 nm, gradient B 20 → 60% (30 min)) t_R = 17.2 min, purity 99.2%. $\lambda_{max.}$, EtOH (lgε): 261 (4.4), 479 nm (4.0). ν_{max}: 1615, 1584, 1462, 1419, 1351, 1301, 1166, 1044, 1021, 968 cm^{-1}. ^1H NMR (400 MHz, DMSO-d_6, 23 °C) δ 13.90 (1H, s, OH); 13.70 (1H, s, OH); 8.26 (2H, m, H-6,7); 8.07 (3H, br. s, NH_3); 7.96 (2H, m, H-8,9); 3.93 (1H, m, NCH_2); 3.82 (1H, m, NCH_2); 3.75 (1H, m, NCH); 3.55 (2H, m, NCH_2); 2.55 (3H, s, Me); 2.32 (3H, s, SMe); 2.25 (1H, m, CH_2CH_2CH); 2.00 (1H, m, CH_2CH_2CH). ^{13}C NMR (400 MHz, DMSO-d_6, 23 °C) δ 184.07, 183.94 (C = O); 183.90, 183.91 (C = O); 160.82, 160.72 (N–C = O); 159.03, 158.81 (C); 154.79, 154.64 (C); 147.00 (C); 145.99 (C); 132.20, 132.15 (C); 132.06, 131.98 (C); 124.23, 124.14 (C); 114.76, 114.56 (C); 108.49, 108.39 (C); 107.72, 107.60 (C); 134.52, 134.46 (CH); 134.46, 134.38 (CH); 126.19, 126.11 (CH); 126.01, 125.93 (CH); 50.72, 49.67 (CH); 49.08, 48.57 (CH_2); 45.25, 43.57 (CH_2); 29.88, 28.23 (CH_2); 39.76 (CH_3); 12.93 (CH_3). HRMS (ESI) calculated for $C_{22}H_{19}N_2O_6$ $[M+H]^+$ 407.1238, found 407.1221. Analysis calculated for $C_{22}H_{18}N_2O_6{}^*CH_4O_3S{}^*2H_2O$, %: C 51.30, H 4.87, N 5.20. Found, %: 51.64, H 4.67, N 5.13.

4.1.7. (S)-3-(3-Aminopyrrolidine-1-carbonyl)-4,11-dihydroxy-2-methylanthra [2,3-b]furan-5,10-dione methanesulfonate (**3d**)

This compound was prepared from **6** and (*S*)-3-(Boc-amino) pyrrolidine as described for **3a**. An orange-reddish powder, yield 74%, mp 327–328 °C (dec.). HPLC (LW = 260 nm, gradient B 20 → 60% (30 min)) t_R = 17.2 min, purity 96.9%. $\lambda_{max.}$, EtOH (lgε): 261 (4.4), 479 nm (4.0). ν_{max}: 1615, 1584, 1462, 1419, 1351, 1301, 1166, 1044, 1021, 968 cm^{-1}. ^1H NMR (400 MHz, DMSO-d_6, 107 °C) δ 10.13 (3H, br. s, NH_3); 8.18 (2H, br. s, H-6,7); 7.87 (2H, br. s, H-8,9); 3.94–3.42 (5H, br. m, CH_2NCH_2CH); 2.54 (3H, s, Me); 2.41 (3H, s, SMe); 2.33 (1H, br. s, CH_2CH_2CH); 2.08 (1H, br. s, CH_2CH_2CH). ^{13}C NMR (400 MHz, DMSO-d_6, 107 °C) δ 183.09 (C = O); 182.90 (C = O); 160.36 (N–C = O); 158.33; 155.48; 147.99; 146.27; 132.27 (2C); 124.18; 114.52; 108.51; 107.73; 133.99 (CH); 133.93 (CH); 125.88 (CH); 125.78 (CH); 50.11, 49.23 (CH); 48.51, 48.35 (CH_2); 44.77, 42.94 (CH_2); 29.20, 27.86 (CH_2); 39.20 (CH_3); 12.22 (CH_3). HRMS (ESI) calculated for $C_{22}H_{19}N_2O_6$ $[M+H]^+$ 407.1238, found 407.1230. Analysis calculated for $C_{22}H_{18}N_2O_6{}^*CH_4O_3S{}^*2H_2O$, %: C 51.30, H 4.87, N 5.20. Found, %: 51.53, H 4.76, N 5.10.

4.1.8. 4,11-Dihydroxy-2-methyl-5,10-dioxo-N-(piperidin-3-yl)-5,10-dihydroanthra [2,3-b]furan-3-carboxamide methanesulfonate (**3e**)

This compound was prepared from **6** and (*R,S*)-1-Boc-3-aminopiperidine as described for **3a**. A red powder, yield 71%, mp 314–316 °C (dec.). HPLC (LW = 260 nm, gradient B 20 → 60% (30 min)) t_R = 22.28 min, purity 97.3%. $\lambda_{max.}$, EtOH (lgε): 261 (4.4), 479 nm (4.0). ^1H NMR (400 MHz, DMSO-d_6, 23 °C) δ 14.55 (1H, br. s, OH); 13.58 (1H, br. s, OH); 8.68 (3H, br. s, CONH, NH_2); 8.15 (2H, m, H-6,7); 7.89 (2H, br. s, H-8,9); 4.13 (1H, m, CH); 3.40 (1H, m, $(CH_2)_2N$); 3.24 (1H, m, $(CH_2)_2N$); 2.89 (2H, m, $(CH_2)_2N$); 2.64 (3H, s, Me); 2.35 (3H, s, SMe); 1.95 (2H, m, CH_2); 1.76 (1H, m, CH_2); 1.61 (1H, m, CH_2). ^{13}C NMR (400 MHz, DMSO-d_6, 70 °C) δ 182.03 (C = O); 181.98 (C = O); 163.13 (N–C = O); 160.29; 157.50; 149.32; 146.64; 132.26; 132.11; 123.49; 114.24; 108.40; 107.70; 134.31 (CH); 134.29 (CH); 126.17 (CH); 126.00 (CH); 45.95 (CH); 43.30 (CH_2); 42.84 (CH_2); 27.33 (CH_2); 20.30 (CH_2); 39.40 (CH_3); 13.48 (CH_3). HRMS (ESI) calculated for $C_{23}H_{21}N_2O_6$ $[M+H]^+$ 421.1394, found 421.1385.

4.1.9. 3-(3-Aminopiperidine-1-carbonyl)-4,11-dihydroxy-2-methylanthra [2,3-b]furan-5,10-dione methanesulfonate (**3f**)

This compound was prepared from **6** and (*R,S*)-3-(Boc-amino) piperidine as described for **3a**. A red powder, yield 73%, mp 331–332 °C °C (dec.). HPLC (LW = 260 nm, gradient B 20 → 60% (30 min)) t_R = 19.18 min, purity 98.1%. $\lambda_{max.}$, EtOH (lgε): 261 (4.4), 479 nm (4.0). ν_{max}: 1643, 1613, 1581, 1479, 1455,1421, 1346, 1301, 1169, 1048, 1021, 963 cm^{-1}. ^1H NMR (400 MHz, DMSO-d_6, 23 °C) δ 13.90 (1H, br. s, OH); 13.67 (1H, br. s, OH); 8.25 (2H, m, H-6,7); 8.05 (2H, br. s, NH_2); 7.96 (2H, m, H-8,9); 7.73 (1H, d, J = 11.4 Hz, CONH); 4.77–4.51 (1H, m, $(CH_2)_2N$); 3.99–3.69 (1H, m, $(CH_2)_2N$); 5.50 (1H, m, CH); 3.20–2.99 (2H, m, $(CH_2)_2N$); 2.54 (3H, m, Me); 2.32 (3H, s, SMe); 2.05–1.85 (2H, m, CH_2); 1.59–1.54 (2H, m, CH_2). ^{13}C NMR (400 MHz, DMSO-d_6, 90 °C) δ 183.19 (C = O); 182.98 (C = O); 161.05 (N–C = O); 157.64; 155.48; 148.02; 146.36; 132.33 (2C); 124.60; 113.54; 108.58; 107.80; 134.07 (CH); 134.01 (CH); 125.85 (CH); 125.80 (CH); 48.26, 46.56 (CH); 45.99 (CH_2); 43.59, 40.84 (CH_2); 27.78, 27.55 (CH_2); 22.57, 21.13 (CH_2); 39.22 (CH_3); 12.14 (CH_3). HRMS (ESI) calculated for $C_{23}H_{21}N_2O_6$ $[M+H]^+$ 421.1394, found 421.1390.

4.1.10. 4,11-Dihydroxy-2-methyl-5,10-dioxo-N-(piperidin-4-yl)-5,10-dihydroanthra [2,3-b]furan-3-carboxamide methanesulfonate (**3g**)

This compound was prepared from **6** and 1-Boc-4-aminopiperidine as described for **3a**. A red powder, yield 76%, mp

332–334 °C °C (dec.). HPLC (LW = 260 nm, gradient B 20 → 60% (30 min)) t_R = 20.62 min, purity 98.0%. $\lambda_{max.}$, EtOH (lgε): 261 (4.4), 481 nm (4.0). ν_{max}: 3031, 1650, 1617, 1580, 1457, 1354, 1306, 1228, 1159, 1043, 964 cm^{-1}. ^{1}H NMR (400 MHz, DMSO-d_6, 23 °C) δ 14.62 (1H, br. s, OH); 13.69 (1H, br. s, OH); 8.62 (1H, d, J = 7.1 Hz, CONH); 8.55 (1H, br. s, NH_2); 8.33 (1H, br. s, NH_2); 8.25 (2H, m, H-6,7); 7.95 (2H, m, H-8,9); 4.11 (1H, m, CH); 3.32 (2H, m, $(CH_2)_2N$); 3.12 (2H, m, $(CH_2)_2N$); 2.67 (3H, s, Me); 2.36 (3H, s, SMe); 2.08 (2H, m, CH_2); 1.78 (2H, m, CH_2). ^{13}C NMR (400 MHz, DMSO-d_6, 107 °C) δ 182.26 (2C = O); 162.64 (N–C = O); 160.12; 157.62; 149.25; 146.59; 132.19; 132.11; 123.81; 114.76; 108.38; 107.72; 134.44 (2CH); 126.23 (CH); 126.11 (CH); 43.58 (CH); 41.71 (2CH_2); 27.55 (2CH_2); 39.30 (CH_3); 13.44 (CH_3). HRMS (ESI) calculated for $C_{23}H_{21}N_2O_6$ $[M+H]^+$ 421.1394, found 421.1402.

4.1.11. 3-(4-Aminopiperidine-1-carbonyl)-4,11-dihydroxy-2-methylanthra [2,3-b]furan-5,10-dione methanesulfonate (**3h**)

This compound was prepared from **6** and 4-(Boc-amino)piperidine as described for **3a**. A red powder, yield 70%, mp 335–337 °C °C (dec.). HPLC (LW = 260 nm, gradient B 20 → 60% (30 min)) t_R = 17.8 min, purity 98.3%. $\lambda_{max.}$, EtOH (lgε): 261 (4.4), 479 nm (4.0). ^{1}H NMR (400 MHz, DMSO-d_6, 23 °C) δ 13.80 (1H, br. s, OH); 13.46 (1H, br. s, OH); 8.28 (2H, br. s, H-6,7); 7.97 (2H, br. s, H-8,9); 7.91 (3H, br. s, NH_3); 4.62 (1H, d, J = 13.4 Hz, CH); 3.64 (1H, m, $CON(CH_2)_2$); 3.40 (1H, t, J = 14.0 Hz, $CON(CH_2)_2$); 3.18 (1H, m, $CON(CH_2)_2$); 2.91 (1H, t, J = 10.0 Hz, $CON(CH_2)_2$); 2.54 (3H, s, Me); 2.32 (3H, s, SMe); 2.05 (1H, m, CH_2); 1.80 (1H, m, CH_2); 1.64–1.36 (2H, m, CH_2). HRMS (ESI) calculated for $C_{23}H_{21}N_2O_6$ $[M+H]^+$ 421.1394, found 421.1399.

4.1.12. 4,11-Dihydroxy-2-methyl-3-(piperazine-1-carbonyl)anthra [2,3-b]furan-5,10-dione methanesulfonate (**3i**)

This compound was prepared from **6** and 1-Boc-piperazine as described for **3a**. A red powder, yield 71%, mp > 350 °C (dec.). HPLC (LW = 260 nm, gradient B 20 → 60% (30 min)) t_R = 18.1 min, purity 99.2%. $\lambda_{max.}$, EtOH (lgε): 261 (4.4), 479 nm (4.0). ν_{max}: 1642, 1613, 1577, 1477, 1420, 1380, 1307, 1183, 1041, 1023, 1006, 968 cm^{-1}. ^{1}H NMR (400 MHz, DMSO-d_6, 23 °C) δ 13.77 (2H, br. s, OH); 8.85 (2H, br. s, NH_2); 8.24 (2H, m, H-6,7); 7.94 (2H, m, H-8,9); 3.95 (1H, m, $CON(CH_2)_2$); 3.83 (1H, m, $CON(CH_2)_2$); 3.56 (2H, m, $CON(CH_2)_2$); 3.25 (2H, m, $(CH_2)_2N$); 3.10 (1H, m, $(CH_2)_2N$); 3.05 (1H, m, $(CH_2)_2N$); 2.54 (3H, s, Me); 2.33 (3H, s, SMe). ^{13}C NMR (400 MHz, DMSO-d_6, 70 °C) δ 184.22 (C = O); 184.05 (C = O); 161.13 (N–C = O); 158.85; 154.88; 147.55; 146.47; 132.73; 132.68; 124.40; 112.93; 108.98; 108.21; 134.58 (CH); 134.55 (CH); 128.36 (CH); 126.30 (CH); 43.09 (CH_2); 42.74 (CH_2); 42.55 (CH_2); 39.26 (CH_3); 38.22 (CH_2); 12.52 (CH_3). HRMS (ESI) calculated for $C_{22}H_{19}N_2O_6$ $[M+H]^+$ 407.1238, found 407.1224.

4.1.13. 4,11-Dihydroxy-2-methyl-3-(2-methylpiperazine-1-carbonyl)anthra [2,3-b]furan-5,10-dione methanesulfonate (**3j**)

This compound was prepared from **6** and 1-Boc-3-methylpiperazine as described for **3a**. A red powder, yield 69%, mp 345–347 °C (dec.). HPLC (LW = 260 nm, gradient B 20 → 60% (30 min)) t_R = 19.2 min, purity 95.3%. $\lambda_{max.}$, EtOH (lgε): 261 (4.4), 479 nm (4.0). ^{1}H NMR (400 MHz, DMSO-d_6, 23 °C) δ 13.80 (2H, br. s, OH); 9.13 (2H, br. s, NH_2); 8.28 (2H, m, H-6,7); 7.98 (2H, m, H-8,9); 5.01 (1H, m, $CONCH_2$); 4.57 (1H, m, $CONCH_2$); 4.15–4.08 (1H, m, CONCH); 3.61–3.46 (2H, m, $(CH_2)_2N$); 3.25–3.09 (2H, m, $(CH_2)_2N$); 2.55, 2.52 (3H, s, Me); 2.33 (3H, s, SMe); 1.40, 1.23 (3H, m, Me). HRMS (ESI) calculated for $C_{23}H_{21}N_2O_6$ $[M+H]^+$ 421.1394, found 421.1383.

4.1.14. 4,11-Dihydroxy-2-methyl-3-(3-methylpiperazine-1-carbonyl)anthra [2,3-b]furan-5,10-dione methanesulfonate (**3k**)

This compound was prepared from **6** and 1-Boc-2-methylpiperazine as described for **3a**. A red powder, yield 73%, mp > 350 °C (dec.). HPLC (LW = 260 nm, gradient B 20 → 60% (30 min)) t_R = 19.1 min, purity 96.3%. $\lambda_{max.}$, EtOH (lgε): 261 (4.4), 479 nm (4.0). ^{1}H NMR (400 MHz, DMSO-d_6, 23 °C) δ 13.79 (2H, br. s, OH); 8.89 (2H, br. s, NH_2); 8.24 (2H, m, H-6,7); 7.93 (2H, m, H-8,9); 4.62–4.43 (1H, m, $CON(CH_2)_2$); 3.77–3.66 (1H, m, $CON(CH_2)_2$); 3.45–3.39 (2H, m, $CON(CH_2)_2$); 3.20–3.05 (3H, m, $CHNCH_2$); 2.55, 2.51 (3H, s, Me); 2.34 (3H, s, SMe); 1.32, 1.08 (3H, d, J = 6.6 Hz, Me). HRMS (ESI) calculated for $C_{23}H_{21}N_2O_6$ $[M+H]^+$ 421.1394, found 421.1383.

4.1.15. 4,11-Dihydroxy-2-methyl-3-(4-methylpiperazine-1-carbonyl)anthra [2,3-b]furan-5,10-dione methanesulfonate (**3l**)

To a stirring mixture of crude acyl chloride **6** (prepared from acid **5** (100 mg, 0.3 mmol)) in anhydrous chloroform (10 ml) a solution of *N*-methylpiperazine (100 mg, 0.1 mmol)) and pyridine (0.1 ml, 1.1 mmol) in anhydrous chloroform (5 ml) was added. The mixture was refluxed for 5 min, diluted with chloroform (20 ml), washed with water, dried and evaporated. The residue was purified by column chromatography on a silica gel using chloroform-methanol-water-formic acid mixture (10:0:0:0 → 10:3:1:0.2) as an eluting solvent. The red solid obtained after evaporation was dissolved in the mixture of hot water (2 ml) and methane sulfonic acid (0.3 ml, 4.6 mmol). The solution was filtered, the product was precipitated with acetone-ether mixture (3:1). The red solid was collected by filtration, successively washed with acetone, Et_2O, *n*-hexane and dried. The yield of methanesulfonate **3l** was 98 mg (68%) as a red solid, mp > 309–312 °C (dec.). HPLC (LW = 260 nm, gradient B 20 → 60% (30 min)) t_R = 18.8 min, purity 97.1%. $\lambda_{max.}$, EtOH (lgε): 261 (4.4), 479 nm (4.0). ^{1}H NMR (400 MHz, DMSO-d_6, 23 °C) δ 13.94 (1H, br. s, OH); 13.69 (1H, s, OH); 9.76 (1H, br. s, NH); 8.30 (2H, m, H-6,7); 7.97 (2H, m, H-8,9); 4.66 (1H, m, $CON(CH_2)_2$); 3.81 (1H, br. s, $CON(CH_2)_2$); 3.55 (1H, br. s, $CON(CH_2)_2$); 3.44 (1H, br. s, $CON(CH_2)_2$); 3.15 (4H, br. s, $(CH_2)_2N$); 2.88 (3H, s, NMe); 2.54 (3H, s, Me); 2.31 (3H, s, SMe). HRMS (ESI) calculated for $C_{23}H_{21}N_2O_6$ $[M+H]^+$ 421.1394, found 421.1405.

4.1.16. 4,11-Dihydroxy-2-methyl-5,10-dioxo-N-(quinuclidin-3-yl)-5,10-dihydroanthra [2,3-b]furan-3-carboxamide methanesulfonate (**3m**)

This compound was prepared from **6** and 3-aminoquinuclidine hydrochloride as described for **3l**. A red powder, yield 59%, mp 266–267 °C (dec.). HPLC (LW = 260 nm, gradient B 20 → 60% (30 min)) t_R = 22.7 min, purity 97.5%. $\lambda_{max.}$, EtOH (lgε): 261 (4.4), 481 nm (4.0). ν_{max}: 3528, 1658, 1616, 1575, 1461, 1350, 1304, 1220, 1150, 1038, 970 cm^{-1}. ^{1}H NMR (400 MHz, DMSO-d_6, 23 °C) δ 13.67 (2H, br. s, OH); 9.49 (1H, br. s, NH); 8.98 (1H, d, J = 6.0 Hz, NH); 8.21 (2H, m, H-6,7); 7.94 (2H, m, H-8,9); 4.33 (1H, br. s, NCH); 3.76 (1H, t, J = 11.7 Hz, $(CH_2)_3N$); 3.32 (4H, br. s, $(CH_2)_3N$); 3.11 (1H, m, $(CH_2)_3N$); 2.66 (3H, s, Me); 2.31 (3H, s, SMe); 2.23 (1H, m, CH); 2.12 (1H, m, CH_2); 1.96 (2H, m, CH_2); 1.83 (1H, m, CH_2). HRMS (ESI) calculated for $C_{25}H_{23}N_2O_6$ $[M+H]^+$ 447.1551, found 447.1572.

4.2. Cell culture and cytotoxicity assays

The K562 human leukemia cell line (American Type Culture Collection; ATCC, Manassas, VA) and its Pgp-positive subline K562/4 [32] selected for survival in the continuous presence of Dox, the HCT116 colon carcinoma cell line (ATCC) with wild type p53 and the HCT116p53KO subline (both p53 alleles deleted [33]; generated in B.Vogelstein lab, Johns Hopkins University, Baltimore, MD) were cultured in Dulbecco modified Eagle's medium supplemented with

5% fetal calf serum (HyClone, Logan, UT), 2 mM L-glutamine, 100 U/ml penicillin, and 100 μg/ml streptomycin. The murine leukemia L1210 and human T-lymphocyte Molt4/C8 cell line (ATCC) were propagated in RPMI-1640 supplemented with 10% fetal calf serum, 0.075% $NaHCO_3$ and 2 mM L-glutamine, 100 U/ml penicillin, and 100 μg/ml streptomycin at 37 °C, 5% CO_2 in a humidified atmosphere. The hFB-hTERT6 skin fibroblasts (obtained via a lentiviral transduction of full-length TERT gene under a CMV promoter (generated in Engelhardt Institute of Molecular Biology; gift of E. Dashinimaev) were cultured in Dulbecco modified Eagle's medium supplemented with 5% fetal calf serum, 2 mM L-glutamine, 100 U/ml penicillin, and 100 μg/ml streptomycin. Cells in logarithmic phase of growth were used in the experiments. Newly synthesized and reference compounds were dissolved in 10% aqueous DMSO as 10 mM stock solutions followed by serial dilutions in water immediately before experiments. The assays were performed in 96-well microtiter plates. To each well $(5–7.5) \times 10^4$ tumor cells and a given concentration of the tested compound were added. Cells were allowed to proliferate for 48 h (L1210) or 72 h (all other cell lines) at 37 °C in a humidified CO_2-controlled atmosphere. At the end of the incubation period, cells were counted in a Coulter counter. The IC_{50} was defined as the concentration of the compound that inhibited cell proliferation by 50%. The assessment of cell viability by MTT test has been reported by us [10]. Cell cycle distribution and Annexin V-propidium iodide staining were performed as described [34].

4.3. Intracellular drug accumulation assays

The K562 or K562/4 cells (5×10^5 in 3 ml of culture medium) were treated with 1 μM Dox, **3c** or **3d** for indicated time intervals, pelleted, washed with ice cold saline, resuspended in saline on ice and immediately analyzed by flow cytometry on a BD FACSCanto II (BD Biosciences, USA) in the PE channel (575/26 nm). Values of MFC were calculated from cell fluorescence histograms after the acquisition of at least 10,000 single cell events. Background fluorescence of untreated cells was subtracted from each group. Data were analyzed using FACSDiva program (BD Biosciences).

4.4. Drug-DNA complex formation

The binding of compounds **3c** and **3d** to ctDNA was determined in 100 mM KCl, 10 mM Na phosphate buffer pH 6.0 at 20 °C. Absorbance spectra were recorded with Jasco V550 spectrophotometer (Jasco, Japan). Fluorescence spectra were recorded with Cary Eclipse fluorescence spectrophotometer (Varian Inc, USA; excitation 490 nm, emission 500–700 nm). The concentration of ctDNA (double stranded; moles of bp) was determined in a sodium phosphate buffered solution at 20 °C using the molar extinction coefficient $\varepsilon[\text{ctDNA}] = 13200\ \text{M(bp)}^{-1}\ \text{cm}^{-1}$. Binding constants were determined by McGee-von Hippel approximation of binding isoterms in Scatchard coordinates.

4.5. Molecular docking

The 3D models of the ligands were built using SYBYL X1.2 molecular graphics software package (Tripos Inc., St. Louis, MI). Search of geometry for the models of ligand conformation with the smallest energy and calculation of electron density distribution were performed based on density functional theory (DFT) hybrid exchange-correlation functional B3LYP (Becke three-parameter (exchange); Lee, Yang and Parr (correlation)) [35] with basic sets 6-31G++2d,2p. After that, to calculate partial atomic charges, Natural population analysis (NPA) [36,37] scheme was used. All quantum mechanics simulations were carried out using Gaussian 09 program [38].

The coordinates for 3D models of targets were taken from PDB: 2DES for DNA and 4A3F for protein. The 3D models of the targets were created with Molsoft ICM version 3.8–3 [39,40]. During this process the following procedures were performed: adding hydrogen atoms and missing a heavy atom in the amino acid side groups, assignment of atom types and charges from force field ECEPP/3 [41], estimating the charged state of all His, Asp, Glu, Arg, Lys, and Cys residues, and the sugar-phosphate backbone in DNA taking into account pH 7.0, imposition of internal coordinates tree on the original pdb coordinates, and MM optimization using conjugate gradient minimization was done to eliminate minor van der Waals clashes of atoms.

To define the most probable binding site of ligands on the target surface, the procedure of flexible ligand docking was performed with Molsoft ICM. For the docking process 3D models of ligands were converted into an ICM object. Docking on the protein kinase surface was carried out in the domain containing the active site and neighboring amino acids located around a 10 Å radius vicinity. For both targets a rigid target docking was performed with application of grid potential. The energy parameters were: E_{Hvw} is van der Waals for carbon probe, E_{Cvw} for hydrogen probe, E_{hp} is hydrophobic (proportional to the buried hydrophobic surface area), E_{el} is electrostatic (computed by the Coulomb formula with distance dependent dielectric constant (4^*r_{ij}) and partial atomic charges of the targets were corrected by charge quantity transferred to solvent and estimated by solving the Poisson equation with application of boundary element method); E_{hb} is hydrogen bonding (calculated as spherical Gaussians centered at the ideal putative donor and/or acceptor sites). Each aforementioned target was represented by pre-calculated potential grid maps with 0.5 Å grid step. Search for possible positions of ligands on the target surface was realized using biased probability Monte Carlo (BPMC) minimization procedure [42], involving a random change of the positional variables and intramolecular variables of the ligand followed by local energy minimization (1000 steps quasi-Newton method) and selection by the Metropolis criterion. BPMC procedure was performed from multiple starting points. The energy estimation used during each BPMC procedure was performed by the formula:

$$E = E_{Hvw} + E_{Cvw} + 2.16E_{el} + 2.53E_{hb} + 4.35E_{hp} + 0.2E_{solv}$$

During each BPMC procedure the solvation energy E_{solv}, calculated with application of atomic solvent accessible surfaces (ASA) model, was added after local energy optimization. For complexes of the ligand with the protein kinase obtained in the initial rigid body docking were further refined by optimizing the conformation of side chain amino acids located in 4 Å radius vicinity of the ligand with BPMC procedure. At this stage, during each BPMC procedure the energy was calculated as

$$E = E_{int} + E_{Hvw} + E_{Cvw} + 2.16E_{el} + 2.53E_{hb} + 4.35E_{hp} + 0.2E_{solv}$$

The internal energy E_{int} included internal van der Waals interactions, hydrogen bonding and torsion energy calculated with ECEPP/3 parameters, and the Coulomb electrostatic energy with distance dependent dielectric constant (4^*r_{ij}). Finally, for each target, the conformational stacks obtained from docking were sorted by energy, and 100 best conformations were selected for accurate estimation of energy of binding. From the conformations obtained in the docking to DNA we selected the ones with the geometry on the target surface similar to the position of the ligand in the complex (PDB: 2DES [43]). We used this criteria assuming that the similarity of structures of ligands should provide similarity of the ways of their binding to DNA. In case of docking into the protein

kinase surface, in addition to the binding energy, a steric factor (i.e., the ability to penetrate into the cavity formed by the active center) was used as the second criterion. Since the estimation of electrostatic free energy in the docking procedure was rather simple, it was carried out more rigorously using REBEL method [44]. As the values of energies of van der Waals interactions and the values of hydrogen bond energies for individual molecules of targets and ligands and for the target-ligand complexes are close in aqueous environment, for estimation of binding energy (in case of DNA) the sum of electrostatic and hydrophobic components was used. In case of the protein kinase, the loss of configurational entropy of the side chains of amino acid residues was added to this sum. The hydrophobic component was calculated as a product of the total solvent accessible area by the surface tension parameter (0.012 kcal/(mol*$Å^2$). According to recommendations of ICM developers, the dielectric constants of the targets, the ligands and the complexes were taken as 12.7; the respective parameter for implicit water was 78.5. Graphical representation and calculation of hydrophobic potential partition on the surface of targets were performed with SYBYL X 1.2.

4.6. Top1/Top2 DNA relaxation assays and Top1 mediated DNA cleavage reactions

One or two units of purified Top1 (Promega, USA) were incubated with 250 ng of supercoiled pBR322 plasmid DNA (Fermentas, Lithuania) in the buffer (35 mM Tris-HCl, pH 8.0; 72 mM KCl, 5 mM $MgCl_2$, 5 mM dithiotreitol, 2 mM spermidine, 100 μg/ml bovine serum albumin) in the presence of 0.1% DMSO (vehicle control; Fig. 8A, lane Top1) or tested compounds at 37 °C for 30 min. For Top2 activity assays, 250 ng of supercoiled pBR322 plasmid and 4 units of purified enzyme (TopoGen, USA) were incubated in the buffer (50 mM Tris-HCl, pH 8.0; 150 mM NaCl, 10 mM $MgCl_2$, 0.5 mM dithiothreitol, 30 μg/ml bovine serum albumin, 2 mM ATP) in the presence of 0.1% DMSO (vehicle control; Fig. 8C, lane Top2) or tested compounds at 37 °C for 30 min. The reactions were terminated by the addition of sarcosyl (up to 1%). Then proteinase K was added (final concentration 50 μg/ml), and the reaction mixtures were incubated for 30 min (Top1) or 15 min (Top2) at 37 °C. DNA topoisomers were resolved by electrophoresis in 1% agarose gel (3 h, 70 V) in the buffer containing 40 mM Tris base, 1 mM EDTA and 30 mM glacial acetic acid. Gels were stained with ethidium bromide after electrophoresis.

DNA cleavage reactions were performed as described [12,45] with a DNA substrate consisting of a 117 bp oligonucleotide (Integrated DNA Tech.,) encompassing previously identified Top1 cleavage sites in the 161 bp fragment from pBluescript SK(−) phagemid DNA. The 117 bp oligonucleotide contains a single 5′-cytosine overhang which was 3'end-labeled by fill-in reaction with [^{32}P]dGTP in React 2 buffer (50 mM Tris-HCl, pH 8.0, 100 mM $MgCl_2$, 50 mM NaCl) in the presence of 0.5 units of DNA polymerase I (Klenow fragment, New England BioLabs). Unincorporated [^{32}P]dGTP was removed using mini Quick Spin DNA columns (Roche, Indianapolis, IN). Approximately 2 nM of radiolabeled DNA substrate was incubated with recombinant Top1 in 20 μl of the reaction buffer (10 mM Tris-HCl pH 7.5, 50 mM KCl, 5 mM $MgCl_2$, 0.1 mM EDTA, and 15 μg/ml bovine serum albumin) at 25 °C for 20 min with indicated concentrations of compounds. Reactions were terminated by sodium dodecyl sulphate (0.5% final concentration) followed by the addition of two volumes of the loading dye (80% formamide, 10 mM sodium hydroxide, 1 mM sodium EDTA, 0.1% xylene cyanol, and 0.1% bromophenol blue). Aliquots of reaction mixtures were subjected to 20% denaturing polyacrylamide gel electrophoresis. Gels were dried and visualized with a phosphoimager and ImageQuant software (Molecular Dynamics). For simplicity, cleavage sites were numbered as previously described in the 161 bp fragment [25].

4.7. In vitro kinase assays

The ability of **3d** to influence the activity of human protein kinases was tested by ProQinase GMBH (Freiburg, Germany) according to the company's standard protocol (^{33}PanQinase®Activity Assay). The full panel of tested protein kinases is presented in Supplement Material.

4.8. Animals and in vivo tumor models

The DBA2 or BDF_1[DBA_2 x $C_{57}Bl_6$] conventional mice (female, 19–21 g) were bred and supported in the animal department at FSBSI « N.N.Blokhin Cancer Research Center» of the Ministry of Health of the Russian Federation. Animals were given food and water *ad libitum*. P388 leukemia cells (10^6 per animal) were transplanted i.p. according to the published protocol [46]. Compounds **3c**, **3d** or saline (control) were injected into the peritoneal cavity of mice (n = 3–11) daily for 5 days starting on day 1 after tumor inoculation. Animals' weight as well as behavioural and nutritional habits were monitored daily. The minimal criterion of therapeutic efficacy for screening was T/C ≥ 125%. Statistical difference between groups was calculated using Student's *t*-test. Values $p \leq 0.05$ were considered significant [47].

Funding

This study was supported by the Ministry of Industry and Trade of the Russian Federation (state contract 12411.1008799.13.007).

Acknowledgements

The authors thank A. Korolev and N. Maliutina (Gause Institute of New Antibiotics) for HRMS and HPLS analyses; N. Lesnaya, S. Sitdikova and F. Donenko (N.N.Blokhin Cancer Research Center) for assistance in animal experiments; L. van Berckelaer (KU Leuven) for help in cell proliferation assays, M. Petukhov (Konstantinov St. Petersburg Nuclear Physics Institute) for sharing of ICM-equipped computers, and E. Dashinimaev (Engelhardt Institute of Molecular Biology) for immortalized fibroblasts.

Appendix A. Supplementary data

Supplementary data related to this article can be found at http://dx.doi.org/10.1016/j.ejmech.2016.01.050

References

[1] S. Raj, V.I. Franco, S.E. Lipshultz, Anthracycline-induced cardiotoxicity: a review of pathophysiology, diagnosis, and treatment, Curr. Treat. Options Cardiovasc. Med. 16 (2014) 315.
[2] A. Di Marco, M. Gaetani, P. Orezzi, B.M. Scarpinato, R. Silvestrini, M. Soldati, T. Dasdia, L. Valentini, 'Daunomycin', a new antibiotic of the rhodomycin group, Nature 201 (1964) 706–707.
[3] M. Yamamoto, A. Takakura, N. Masuda, Next-generation anthracycline for the management of small cell lung cancer: focus on amrubicin, Drug Des. Devel. Ther. 6 (2009) 189–192.
[4] J. Nadas, D. Sun, Anthracyclines as effective anticancer drugs, Expert Opin. Drug Discov. 1 (2006) 549–568.
[5] M.S. Cookson, S.S. Chang, C. Lihou, T. Li, S.Q. Harper, Z. Lang, R.F. Tutrone, Use of intravesical valrubicin in clinical practice for treatment of nonmuscle-invasive bladder cancer, including carcinoma in situ of the bladder, Ther. Adv. Urol. 6 (2014) 181–191.
[6] A. Marczak, M. Denel-Bobrowska, M. Łukawska, I. Oszczapowicz, Formamidinodoxorubicins are more potent than doxorubicin as apoptosis inducers in human breast cancer cells, Anticancer Res. 35 (2015) 1935–1940.
[7] F.-M. Arcamone, Anthracycline chemistry and biology. II Sabarubicin, Top.

Curr. Chem. 283 (2008) 171–189.
[8] A.E. Shchekotikhin, L.G. Dezhenkova, O.Y. Susova, V.A. Glazunova, Y.N. Luzikov, Y.B. Sinkevich, V.N. Buyanov, A.A. Shtil, M.N. Preobrazhenskaya, Naphthoindole–based analogues of tryptophan and tryptamine: synthesis and cytotoxic properties, Bioorg. Med. Chem. 15 (2007) 2651–2659.
[9] S. Cogoi, S. Zorget, A.E. Shchekotikhin, L.E. Xodo, Potent apoptotic response induced by chloroacetamidineanthrathiophenediones in bladder cancer cells, J. Med. Chem. 58 (2015) 5476–5485.
[10] A.E. Shchekotikhin, V.A. Glazunova, L.G. Dezhenkova, V.F. Traven, J. Balzarini, H.-S. Huang, A.A. Shtil, M.N. Preobrazhenskaya, The first series of 4,11-bis[(2-aminoethyl)amino]anthra[2,3-b]furan-5,10-diones: synthesis and antiproliferative characteristics, Eur. J. Med. Chem. 46 (2011) 423–428.
[11] A.E. Shchekotikhin, A.A. Shtil, Y.N. Luzikov, T.V. Bobrysheva, V.N. Buyanov, M.N. Preobrazhenskaya, 3-Aminomethyl derivatives of 4,11-dihydroxynaphtho[2,3-*f*]indole-5,10-dione for circumvention of anticancer drug resistance, Bioorg. Med. Chem. 13 (2005) 2285–2291.
[12] A.E. Shchekotikhin, V.A. Glazunova, L.G. Dezhenkova, YuN. Luzikov, V.N. Buyanov, H.M. Treshalina, N.A. Lesnaya, V.I. Romanenko, D.N. Kalyuzhny, J. Balzarini, K. Agama, Y. Pommier, A.A. Shtil, M.N. Preobrazhenskaya, Synthesis and evaluation of new antitumor 3-aminomethyl-4,11-dihydroxynaphtho[2,3-*f*]indole-5,10-diones, Eur. J. Med. Chem. 86 (2014) 797–805.
[13] P. Ciapetti, B. Giethlen, Molecular variations based on isosteric replacements, in: C.G. Wermuth (Ed.), The Practice of Medicinal Chemistry, third ed., Academic Press, Boston, MA, 2008, pp. 290–342.
[14] M.V. Gorelik, E.V. Mishina, An interaction of 2,3-dichloro- and 2-chloro-1,4-dihydroxyanthraquinones with carboanions, Zh. Org. Khim 19 (1983) 2185–2191.
[15] S. Kim, M. Matsuoka, Y. Kubo, T. Yodoshi, T. Kitao, Novel syntheses of anthraquinonoid near-infrared absorbing dyes, Dyes Pigm 7 (1986) 93–102.
[16] D.M. Pawar, A.A. Khalil, D.R. Hooks, K. Collins, T. Elliott, J. Stafford, L. Smith, E.A. Noe, E and Z conformations of esters, thiol esters, and amides, J. Am. Chem. Soc. 120 (1998) 2108–2112.
[17] P.A. Ottersbach, G. Schnakenburg, M. Gütschow, Atropisomerism in azadipeptides: evaluation of N1-methylation and thioamide introduction, Tetrahedron Lett. 56 (2015) 4889–4891.
[18] A. Ahmed, R.A. Bragg, J. Clayden, L.W. Lal, C. McCarthy, J.H. Pink, N. Westlund, S.A. Yasin, Barriers to rotation about the chiral axis of tertiary aromatic amides, Tetrahedron 54 (1998) 13277–13294.
[19] D.B. Khadka, W.J. Cho, Topoisomerase inhibitors as anticancer agents: a patent update, Expert Opin. Ther. Pat. 23 (2013) 1033–1056.
[20] J.D. McGhee, P.H. von Hippel, Theoretical aspects of DNA–protein interactions: co-operative and non-co-operative binding of large ligands to a one-dimensional homogeneous lattice, J. Mol. Biol. 86 (1974) 469–489.
[21] S.R. Byrn, G.D. Dolch, Analysis of binding of daunorubicin and doxorubicin to DNA using computerized curve-fitting procedures, J. Pharm. Sci. 67 (1978) 688–693.
[22] S.B. Howerton, A. Nagpal, L.D. Williams, Surprising roles of electrostatic interactions in DNA–ligand complexes, Biopolymers 69 (2003) 87–99.
[23] G.E. Kellogg, J.N. Scarsdale, F.A. Fornari Jr., Identification and hydropathic characterization of structural features affecting sequence specificity for doxorubicin intercalation into DNA double-stranded polynucleotides, Nucl. Acids Res. 26 (1998) 4721–4732.
[24] S. Antony, M. Jayaraman, G. Laco, G. Kohlhagen, K.W. Kohn, M. Cushman, Y. Pommier, Differential induction of topoisomerase I-DNA cleavage complexes by the indenoisoquinoline MJ-III-65 (NSC 706744) and camptothecin: base sequence analysis and activity against camptothecin-resistant topoisomerases I, Cancer Res. 63 (2003) 7428–7435.
[25] P. Pourquier, L.-M. Ueng, J. Fertala, D. Wang, H.-K. Park, J.M. Essigmann, M.-A. Bjornsti, Y. Pommier, Induction of reversible complexes between eukaryotic DNA topoisomerase I and DNA-containing oxidative base damages 7,8-dihydro-8-oxoguanine and 5-hydroxycytosine, J. Biol. Chem. 274 (1999) 8516–8523.
[26] A. Wehenkel, P. Fernandez, M. Bellinzoni, V. Catherinot, N. Barilone, G. Labesse, M. Jackson, P. Alzari, The structure of PknB in complex with mitoxantrone, an ATP-competitive inhibitor, suggests a mode of protein kinase regulation in mycobacteria, FEBS Lett. 580 (2006) 3018–3022.
[27] S.W. Huang, J.C. Lien, S.C. Kuo, T.F. Huang, PPemd26, an anthraquinone derivative, suppresses angiogenesis via inhibiting VEGFR2 signalling, Br. J. Pharmacol. 171 (2014) 5728–5742.
[28] E. De Moliner, S. Moro, S. Stefania, G. Zagotto, G. Zanotti, L.A. Pinna, R. Battistutta, Inhibition of protein kinase CK2 by anthraquinone-related compounds. A structural insight, J. Biol. Chem. 278 (2003) 1831–1836.
[29] G. Cozza, L.A. Pinna, S. Moro, Protein kinase CK2 inhibitors: a patent review, Expert Opin. Ther. Pat. 22 (2012) 1081–1097.
[30] Y. Pommier, DNA topoisomerase I inhibitors: chemistry, biology, and interfacial inhibition, Chem. Rev. 109 (2009) 2894–2902.
[31] N.S. Ilyinsky, A.K. Shchyolkina, O.F. Borisova, O.K. Mamaeva, M.I. Zvereva, D.M. Azhibek, M.A. Livshits, V.A. Mitkevich, J. Balzarini, Y.B. Sinkevich, Y.N. Luzikov, L.G. Dezhenkova, E.S. Kolotova, A.A. Shtil, A.E. Shchekotikhin, D.N. Kaluzhny, Novel multi-targeting anthra[2,3-b]thiophene-5,10-diones with guanidine-containing side chains: interaction with telomeric G-quadruplex, inhibition of telomerase and topoisomerase I and cytotoxic properties, Eur. J. Med. Chem. 85 (2014) 605–614.
[32] A. Shtil, T. Grinchuk, E. Mechetner, T. Ignatova, Overexpression of the MDR1 gene in associated with a decreased mitochondrial transmembrane potential in K562 human leukemia cells selected for P-glycoprotein-mediated multidrug resistance, Int. J. Oncol. 17 (2000) 387–392.
[33] F. Bunz, A. Dutriaux, C. Lengauer, T. Waldman, S. Zhou, J.P. Brown, J.M. Sedivy, K.W. Kinzler, B. Vogelstein, Requirement for p53 and p21 to sustain G2 arrest after DNA damage, Science 282 (1998) 1497–1501.
[34] L.N. Lysenkova, K.F. Turchin, A.M. Korolev, E.E. Bykov, V.N. Danilenko, O.B. Bekker, A.S. Trenin, S.M. Elizarov, L.G. Dezhenkova, A.A. Shtil, M.N. Preobrazhenskaya, A novel acyclic oligomycin A derivative formed via retro-aldol rearrangement of oligomycin A, J. Antibiot. 65 (2012) 405–411.
[35] C. Lee, W. Yang, R.G. Parr, Development of the Colle-Salvetti correlation-energy formula into a functional of the electron density, Phys. Rev. B Condens. Matter 37 (1988) 785–789.
[36] A.E. Reed, F. Weinhold, Natural bond orbital analysis of near-Hartree-Fock water dimer, J. Chem. Phys. 78 (1983) 4066–4073.
[37] A.E. Reed, R.B. Weinstock, F. Weinhold, Natural-population analysis, J. Chem. Phys. 83 (1985) 735–746.
[38] M.J. Frisch, G.W. Trucks, H.B. Schlegel, G.E. Scuseria, M.A. Robb, J.R. Cheeseman, G. Scalmani, V. Barone, B. Mennucci, G.A. Petersson, H. Nakatsuji, M. Caricato, X. Li, H.P. Hratchian, A.F. Izmaylov, J. Bloino, G. Zheng, J.L. Sonnenberg, M. Hada, M. Ehara, K. Toyota, R. Fukuda, J. Hasegawa, M. Ishida, T. Nakajima, Y. Honda, O. Kitao, H. Nakai, T. Vreven, J.A. Montgomery Jr., J.E. Peralta, F. Ogliaro, M. Bearpark, J.J. Heyd, E. Brothers, K.N. Kudin, V.N. Staroverov, R. Kobayashi, J. Normand, K. Raghavachari, A. Rendell, J.C. Burant, S.S. Iyengar, J. Tomasi, M. Cossi, N. Rega, J.M. Millam, M. Klene, J.E. Knox, J.B. Cross, V. Bakken, C. Adamo, J. Jaramillo, R. Gomperts, R.E. Stratmann, O. Yazyev, A.J. Austin, R. Cammi, C. Pomelli, J.W. Ochterski, R.L. Martin, K. Morokuma, V.G. Zakrzewski, G.A. Voth, P. Salvador, J.J. Dannenberg, S. Dapprich, A.D. Daniels, O. Farkas, J.B. Foresman, J.V. Ortiz, J. Cioslowski, D.J. Fox, Gaussian 09, Revision A.1, Gaussian, Inc., Wallingford CT, 2009.
[39] R. Abagyan, M. Totrov, D. Kuznetsov, ICM, a new method for protein modeling and design: applications to docking and structure prediction from the distorted native conformation, J. Comput. Chem. 15 (1994) 488–506.
[40] M. Totrov, R. Abagyan, Flexible protein-ligand docking by global energy optimization in internal coordinates, Proteins Suppl. 1 (1997) 215–220.
[41] Y.A. Arnautova, A. Jagielska, H.A. Scheraga, A new force field (ECEPP-05) for peptides, proteins, and organic molecules, J. Phys. Chem. B 110 (2006) 5025–5044.
[42] R. Abagyan, M. Totrov, Biased probability Monte Carlo conformational searches and electrostatic calculations for peptides and proteins, J. Mol. Biol. 235 (1994) 983–1002.
[43] M. Cirilli, F. Bachechi, G. Ughetto, F.P. Colonna, M.L. Capobianco, Interactions between morpholinyl anthracyclines and DNA. The crystal structure of a morpholinodoxorubicin bound to d(CGTACG), J. Mol. Biol. 230 (1993) 878–889.
[44] M. Totrov, R. Abagyan, Rapid boundary element solvation electrostatics calculations in folding simulations: successful folding of a 23-residue peptide, Biopolymers 60 (2001) 124–133.
[45] T.S. Dexheimer, Y. Pommier, DNA cleavage assay for the identification of topoisomerase I inhibitors, Nat. Prot. 3 (2008) 1736–1750.
[46] T. Balandin, E. Edelweis, N. Andronova, H. Treshalina, A. Sapozhnikov, S. Deev, Antitumor activity and toxicity of anti-HER2 immunoRNase scFv 4D5-dibarnase in mice bearing human breast cancer xenograft, Invest. New Drugs 29 (2011) 22–32.
[47] Anticancer Drug Development Guide, in: B.A. Teicher, P.A. Andrews (Eds.), Preclinical Screening, Clinical Trials, and Approval, second ed., Humana Press, 2004, p. 450.